Doctoral Thesis

Studies on Anomalies in the Third Derivatives of Gibbs Energy in Aqueous Solutions of Organic Compounds

---

Koh Yoshida

Research Center for Structural Thermodynamics
Department of Chemistry
Graduated School of Science
Osaka University

February 2015

Acknowledgement

This work would not have been completed without help and support of many individuals. I would like to thank everyone who has helped me along the way. Particularly:

Prof. Akira Inaba, Prof Yasuhiro Nakazawa, and Prof. Motohiro Nakano (Osaka University) for providing me an opportunity to conduct my doctoral research under them and for support over the course of it.

Dr. Yoshikata Koga (University of British Columbia) for a number of valuable advice and helpful suggestions, and correcting this thesis.

Prof. Peter Westh (Saurashtra University) for use and advice of titration calorimeter.

Prof. Ken-ichi Tozaki (Chiba University) for making the apparatus and the programs of differential pressure perturbation calorimeter.

The members of the Research Center for Structural Thermodynamics and my collage friends for all memorable times.

Lastly, my family without whose support none of this would have been possible.

Abstract

The higher order derivatives of excess Gibbs energy, G^{E}, than commonly used were obtained in aqueous solutions of a number of non-electrolytes in order to study the "Mixing Scheme", or the molecular level scenario of mixing. For tetrahydrofuran (THF) aqueous solution, the enthalpic and entropic THF-THF interactions, $H^{E}_{THF\text{-}THF}$ and $TS^{E}_{THF\text{-}THF}$, defined in the text, show broad peak-type anomalies. On the other hand, the volumetric THF-THF interaction $V^{E}_{THF\text{-}THF}$, and the partial molar entropy-volume cross fluctuation density, ${}^{SV}\delta_{THF}$, both being third derivatives of G^{E}, have a bend first followed by a weak peak anomalies. This pattern difference between the different third derivatives is similar to that for methanol. It is, therefore, suggested that THF is an amphiphile together with methanol.

The temperature dependence of ${}^{SV}\delta_{B}$, third derivative, was directly determined in aqueous solutions of solute B. For B, 2-butoxyethanol (BE) and glycerol (Gly) were chosen as representing mono-ol and poly-ol, respectively. ${}^{SV}\delta_{BE}$ in 2-butoxyethanol aqueous solution has a peak-type anomaly, but ${}^{SV}\delta_{Gly}$ in glycerol aqueous solution shows a bend-type anomaly. These different patterns of third derivatives are related to whether the solute in question is hydrophobic or hydrophilic. As temperature increases, the anomalies in these aqueous solution shift towards a lower mole fraction. The relationship between the temperature and the mole fraction at the anomaly forms a single curve which is called as the "Koga line" for each solute. The anomalies of the other third derivative quantities than ${}^{SV}\delta_{B}$ was also on the same curve. The Koga line marks

the end of the mixing scheme operative in the H_2O-rich composition region. Extrapolation of the Koga line to the infinite dilution seems to point universally to about 60-80 ˚C, regardless of the identity of solute, hydrophobe or hydrophile. This observation hints that there may be a difference in the molecular organization even for pure liquid water. For pure water, the pressure dependence of pressure derivative of κ_T at fixed temperature, $(\partial\kappa_T/\partial p)_T$, a third derivative of G, shows a gradual bend-type anomaly. As temperature increases, the pressure at the anomaly decreases. Extrapolation of the locus of the anomaly to the atmospheric pressure (0.1 MPa) points to 60-70 ˚C. This coincidence between the two sets of observation indicates that the molecular organization in aqueous solutions below the Koga line and that in pure water below 60-70 ˚C are the same, i.e. the bond percolation of the hydrogen bond network is intact.

Contents

I. Introduction.

It is well known that phase transitions are accompanied by anomalous behaviors of the response functions, heat capacity, compressibility and thermal exapansivity, all being the second derivatives of Gibbs energy. As will be discussed throughout of this thesis, higher order derivatives are sought. Namely, this thesis is concerned with studies of aqueous solutions using the differential approach in solution thermodynamics developed by Koga, [1] and reports my findings on the effect of a solute, tetrahydrofuran, on water. In addition, the nature of aqueous solutions of typically hydrophobic solute 2-butoxyethanol and of typically hydrophilic glycerol were studied in detail, which led to discovery of the Koga Lines for hydrophobic as well as hydrophilic solutes and further to realization of the gradual crossover between the “low-density water” and the "high-density water" in the thermodynamically stable water.

(1) Property of Water

Water has the unique property. For example, water has higher boiling and lower melting points than any other members of hydrides of group XVI elements; H_2S, H_2Se etc., in spite of the fact that the latter hydrides are heavier than water. Water also shows uniqueness in properties of density and expansivity. At 0 ˚C, the density of ice is lower than that of liquid water. In the range of 0-4 ˚C, the volume decreases as temperature increases, that is the expansivity, α_p, is negative.

Water also shows uniqueness in the behaviors of heat capacity, C_p, and compressibility, κ_T. These unique properties are manifestation of its hydrogen bonding capability. For ice the hydrogen bonding network is complete and its structure under ordinary pressure takes ice Ih form with void interstitial spaces due to complete hydrogen bonding. Liquid water, on the other hand, is not so much understood as for ice because the structure of liquid is disordered and fluctuates more vigorously. There have been a number of models for understanding liquid H_2O. To put it crudely, two extreme cases were the mixture model [2], and the bent hydrogen bond model [3]. The former postulates that liquid H_2O is a mixture of two basic components; one is a bulky low-entropy ice-like and the other a dense normal liquid. This model has been developed further by many others, recently by Robinson et al.[4][5][6] In the bent hydrogen bond model, liquid H_2O is regarded as forming a more or less completely hydrogen bonded network with a wide distribution in the hydrogen bond strength due to bending–fluctuating widely. This concept has also been extended, an example being a series of work by Sceates et al. aided by spectroscopic data [7].

Stanley et al. introduce the percolation of hydrogen bond model [8] that reconciles the above two models. It investigates hydrogen-bond connectivity effectively starting with the bent hydrogen bond molecule. It is assumed in this model that hydrogen bonds are randomly distributed; there is no correlation among hydrogen-bond formations. A probability for an arbitrary chosen molecule to have i hydrogen bonds, f_i, is given by a binomial distribution,

$$f_i = {}_4\mathrm{C}_i \, p_\mathrm{b}^{\,i} (1 - p_\mathrm{b})^{\,4-i},$$

where p_b is the probability for an arbitrary chosen pair of the nearest molecules to be hydrogen bonded. A group of four-coordinated water molecules ($i = 4$) is called as "low density water" since an ice-like highly hydrogen bonded region is low in density. This concept covers the idea of the mixture model. If p_b is higher than the percolation threshold (≈ 0.39 for Ih lattice [9]), there exists hydrogen bonding network extended over an entire macroscopic system. They claim that p_b is still high enough that the hydrogen bond network is bond-percolated at the ambient condition. When p_b decreases below the percolation threshold by increasing of temperature or of solute composition, the hydrogen bonding network all over the system is broken and divided into some clusters.

In this thesis, liquid water is understood in this thesis to be an assembly of H_2O molecules by hydrogen bonding. Being liquid, hydrogen bonds are not complete and ordered as in ice, and locally forming and breaking rapidly. Yet the hydrogen bond network is connected throughout the entire bulk of water, i.e. it is bond percolated. [1][8]

(2) Differential Approach in Solution Thermodynamics

The excess Gibbs energy, G^E, provides the holistic information about all the intermolecular interactions in a given system. It is thermodynamically defined as,

$$G^\mathrm{E} = H^\mathrm{E} - TS^\mathrm{E}, \qquad (1)$$

where H^E and S^E are the excess enthalpy and entropy of the system. While, such information is lumped together in G^E, in order to gain more detailed information, it is useful to use derivatives of G^E. The first derivatives of G^E and G^E / T with respect to T at constant pressure and compositions give S^E and H^E as,

$$S^E = - \left(\frac{\partial G^E}{\partial T} \right)_{p, ni} \quad , \tag{2}$$

$$H^E = - T^2 \left(\frac{\partial G^E / T}{\partial T} \right)_{p, ni} . \tag{3}$$

In this manner, the ingredient of G^E in terms of enthalpy and entropy can be isolated. Similarly, the derivatives of G^E with respect to p or n_i are

$$V^E = \left(\frac{\partial G^E}{\partial p} \right)_{T, ni} \quad , \tag{4}$$

$$\mu^E{}_i = \left(\frac{\partial G^E}{\partial n_i} \right)_{T, p} , \tag{5}$$

where V^E is the excess volume, and $\mu^E{}_i$ the excess chemical potential of the i-th substance.

These quantities are first derivatives of G^E. If these first derivatives are differentiated by the molar amount of the i-th component, n_i, the results provide the excess partial molar quantities of i-th component as,

$$S^E{}_i = \left(\frac{\partial S^E}{\partial n_i} \right)_{T, nj \neq i} \quad , \tag{6}$$

$$H^E{}_i = \left(\frac{\partial H^E}{\partial n_i} \right)_{T, nj \neq i} \quad , \tag{7}$$

$$V^{E}_{i} = \left(\frac{\partial V^{E}}{\partial n_i}\right)_{T,\, nj\neq i} \quad , \tag{8}$$

where $n_{j\neq i}$ means holding n_j constant except differentiating n_i. H^{E}_{i}, the excess partial molar enthalpy of i, means the effect of the i-th component on H^{E} of the entire system. Or it signifies the actual enthalpic situation of the i-th component in the mixture under complex intermolecular interactions. Similar physical meanings are applicable for S^{E}_{i} and V^{E}_{i}.

Another set of the second derivatives can be obtained by differentiating G^{E} twice with respect to T and/or p. They correspond to thermodynamic quantities called response functions defined as,

$$C_p \equiv T\left(\frac{\partial S}{\partial T}\right)_{p,\, ni} = -T\left(\frac{\partial^2 G}{\partial T^2}\right)_{p,\, ni} \quad , \tag{9}$$

$$\alpha_p \equiv \frac{1}{V}\left(\frac{\partial V}{\partial T}\right)_{p,\, ni} = \frac{1}{V}\left(\frac{\partial^2 G}{\partial T \partial p}\right)_{ni} \quad , \tag{10}$$

$$\kappa_T \equiv -\frac{1}{V}\left(\frac{\partial V}{\partial T}\right)_{p,\, ni} = -\frac{1}{V}\left(\frac{\partial^2 G}{\partial p^2}\right)_{T,\, ni} \quad , \tag{11}$$

where C_p is isobaric heat capacity, α_p isobaric expansion coefficient, and κ_T isothermal compressibility. This set of second derivatives are related to fluctuation density of entropy and/or volume. [10]

$${}^{S}\delta \equiv \frac{<(S - <S>)^2>}{k_B <V>} = C_p / V, \tag{12}$$

$${}^{V}\delta \equiv \frac{<(V - <V>)^2>}{k_B <V>} = T\kappa_T \,, \tag{13}$$

$${}^{SV}\delta \equiv \frac{<(S - <S>)(V - <V>)>}{k_B <V>} = T\alpha_p \,, \tag{14}$$

where <X> is the average of quantity X. ${}^{S}\delta$ is called as the mean square entropy fluctuation density, ${}^{V}\delta$ the volume fluctuation density, and ${}^{SV}\delta$ is the entropy-volume cross fluctuation density. Thus, it is clear that the higher order derivatives of G have more detailed information of the system.[1]

(3) Second Derivatives for Aqueous Solutions.

The second derivative of G^{E}, $H^{E}_{BE,}$ for aqueous solution of 2-butoxyethanol (BE) is shown in Fig. I-1 at 25 ˚C as an example of mono-ol [11]. At a more dilute region than $x_{BE} = 0.03$, a drastic sigmoidal increase is evident. H^{E}_{Gly} in aqueous solution of glycerol (Gly) is shown in Fig. I-2 as an example for poly-ol aqueous solution at 25 ˚C [12][13]. H^{E}_{Gly} increases also, but in a convex manner in the H_2O-rich region, from $x_{Gly} = 0$ to 0.2. In order to compare the behavior of H^{E}_{B} in these aqueous solutions with that in a non-aqueous system, the values of H^{E}_{B} for the cyclohexane(CH)-benzene(BZ) mixture at 25 ˚C are shown in Fig. I-3. [14] H^{E}_{B}'s for cyclohexane and benzene are positive and show small decrease in the order of 3.5 kJ mol^{-1} in the entire concentration region. This contrasts to 17 kJ increase for 2-butoxyethanol, 5.5 kJ increase for glycerol.

A similar difference is found in another second derivative quantity, ${}^{SV}\delta$. The values of ${}^{SV}\delta$ are shown in Fig. I-4 for 2-butoxyethanol, 1-propanol (1P), and glycerol. [13][15][16] For comparison, ${}^{SV}\delta$ for cyclohexane-benzene mixture is shown in Fig. I-5 calculated from V^{E} data.

[17] These ${}^{SV}\delta$ data were calculated from the α_p data obtained from V^E at two different temperatures. As in the case in H^E_B, the 0.02 decrease in the value of ${}^{SV}\delta$ for non-aqueous system is compared with the increase of 0.8 for 2-butoxyethanol, and of 0.6 for glycerol. Furthermore, the rate of changes as mole fraction increases are apparently different as discussed above. Namely, the results at a dilute region show a sigmoidal increase for 2-butoxyethanol and for 1-propanol. ${}^{SV}\delta$ for glycerol, on the other hand, increases in a convex mode. In comparison, that for cyclohexane-benzene decreases slightly in a concave manner.

The second-derivative differences discussed above between aqueous solutions and benzene-cyclohexane mixture might come from existence or non-existence of hydrogen bond network in solvent. The difference between 2-buxotyethanol and glycerol aqueous solutions might come from the effect of the solute on the hydrogen bonding network. To make these differences stand out more clearly, one more derivatives are taken below.

(4) Third Derivatives of *G*

In order to obtain more sensitive information, the second derivative quantities were differentiated with respect to the molar amount of solute B in a binary system, B and water, (W). The resulting third derivative quantities are defined as,

$$X_{B\text{-}B} = N\frac{\partial X_B}{\partial n_B} = (1 - x_B)\frac{\partial X_B}{\partial x_B}, \tag{15}$$

where $X_{B\text{-}B}$ is the resulting third derivative, X_B the second derivative, N the total molar amount, n_B that of solute B, and x_B the mole fraction of B. $X_{B\text{-}B}$ thus defined signifies the effect of B on X_B. The third derivatives, $X_{B\text{-}B}$, are evaluated graphically without using any fitting functions. Depending on the quality of the second derivative data, the next derivative could be taken numerically using adjacent data points or graphically. Namely, a smooth curve is drawn through all the data points taking possible errors in consideration. Then the value is read off the smooth curve drawn in a fixed increment, δx_{BE}. The partial derivative of the far right of eq. (15) is approximated with the quotient $\delta X_B / \delta x_B$. Such approximation is discussed to be appropriate with a good choice of the size of increment.[18] Thus, the resulting $X_{B\text{-}B}$ data are free from a systematic error due to a wrong choice of the fitting function. Indeed, it is practically impossible to find the correct analytical function for fitting such sharply changing data with an inflection point as shown in Fig. I-1 for 2-butoxyethanol-H_2O.

The $H^E_{B\text{-}B}$ is shown in Fig. I-6 for 2-butoxyethanol (BE) and in Fig. I-7 for glycerol (Gly) aqueous solutions, calculated graphically from Fig. I-1 and I-2. For comparison, $H^E_{B\text{-}B}$ in cyclohexane-benzene mixture are shown in Fig. I-8 calculated from H^E_B data in Fig. I-3. The $H^E_{B\text{-}B}$ in cyclohexane-benzene mixture has no anomaly in the entire range. However, the $H^E_{BE\text{-}BE}$ for aqueous 2-butoxyethanol increases sharply in the dilute region, and shows a peak-type anomaly at point X indicated in Fig I-6. At a larger composition than that at the peak, the gradient changes

at point Y. On the other hand, $H^{E}_{Gly\text{-}Gly}$ for aqueous glycerol decreases in the entire measurement region with two breaks in slope. The ${}^{SV}\delta_B$'s for 2-butoxyethanol and glycerol aqueous solution, and the cyclohexane(CH)-benzene(BZ) mixture are shown in Fig. I-9, I-10, and I-11, respectively. These ${}^{SV}\delta_B$'s were calculated from data in Fig. I-4 and Fig. I-5. The ${}^{SV}\delta_B$ (B = cyclohexane, CH) has no drastic change for cyclohexane-benzene mixture. On the other hand, the same data has a peak-type anomaly for 2-butoxyethanol aqueous solution, and a bend-type anomaly for glycerol aqueous solution. Thus, it is clear that the non-aqueous system is ordinary in that there is one kind of thermodynamic behavior in the entire composition, while the aqueous system seems generally to have a three concentration regions where the thermodynamic behavior, or the molecular level scenario of mixing (that in called the mixing scheme) are qualitatively different, as will be discussed below (see Fig. I-12). This difference could very well be due to the existence of the hydrogen bond network of H_2O. In this thesis, the study on aqueous solutions using the third derivative quantities will be reported.

For third derivative quantities of aqueous solutions, the pattern and the loci of point X and Y are the same for a given class of solute, hydrophobe (BE) or hydrophile (Gly). The same is true for other third derivatives, such as $V^{E}_{B\text{-}B}$.[18] Therefore it seems safe to state that the pattern of third derivatives depend on the hydorphobicity / hydrophilicity of solute. A schematic illustration of relationship between $H^{E}_{B\text{-}B}$ pattern and hydorphobicity / hydrophilicity of solute is shown in Fig.

I-12. For a hydrophobic solute, $H^{E}_{B\text{-}B}$ has a peak-type anomaly as case (a) in Fig. I-12, and for a hydrophilic solute a bend-type anomaly as (d) in the figure. For an amphiphilic solute, the pattern of $H^{E}_{B\text{-}B}$ is intermediate between hydrophobic and hydrophilic solute as case (b) and (c) in Fig. I-12 within the most H_2O-rich region. Therefore from the mole fraction-dependence pattern, the nature of solute in aqueous solutions could be identified as a hydrophobe or hydrophile.

(5) Mixing Schemes in Aqueous Solutions

Using these third derivative data, it became evident that the aqueous solutions generally have three distinct regions where the mixing schemes or the "solution structures" are qualitatively different from those in the other regions. In the H_2O-rich region, H_2O maintains its integrity as liquid water, in that the hydrogen bonding network is at any instance bond-percolated while locally hydrogen bonds are forming / breaking rapidly, i.e. hydrogen bonds are highly fluctuating.[1] In the solute-rich composition, the solute molecules cluster together just as in its pure state. To such clusters, H_2O molecules interact almost as a gas-like single molecule. In the intermediate region, two kinds of clusters mix randomly; one is rich in H_2O, and the other in solute molecules. We call these mixing schemes from the H_2O-rich side as Mixing Scheme I, II, and III (see Fig. I-12). Within Mixing Scheme I, while the integrity of liquid water is maintained, the detailed manner of its modification by the presence of solute depends crucially on the nature

of solute.

From the previous studies on a series of mono-ols with –OH fixed with a varying size of alkyl group, it became apparent that the third derivative quantities of aqueous hydrophobes show peak-type anomalies as discussed above (see Fig. I-6 and I-12). As the size of alkyl groups increases, the peak top becomes higher and the mole fraction locus smaller. From these and other observations using the third derivative quantities it was interpreted that hydrophobic solutes form hydration shells, the hydrogen bond probability within which is net higher slightly than in pure H_2O (i.e. similar to the classical "iceberg formation"[19]), but more importantly the hydrogen bond probability of bulk H_2O away from hydration shells is reduced progressively.[18] As the solute mole fraction increases, the hydrogen bond probability of bulk H_2O away from hydration shells reaches the bond-percolation threshold, and thereupon the hydrogen bonding network is no longer connected throughout. Point X in the Fig. I-6, I-9 and I-12 shows the onset and Y the end of this changeover from Mixing Scheme I to II. Beyond point Y is where Mixing Scheme II is operative. [20][21]

On the other hand, poly-ols behave as hydrophiles due to the presence of multi –OH groups. Fig. I-7 shows $H^{E}_{\text{Gly-Gly}}$. Clearly the behavior of the enthalpic interaction, $H^{E}_{\text{Gly-Gly}}$, in the H_2O-rich region is the opposite for that of BE, shown in Fig. I-6 and I-12 up to point X. This was interpreted as the effect of hydrophiles such that they form hydrogen bonds directly to the existing

hydrogen bond network of H_2O. Thus, they act as impurities in the network. As such, they break H donor / acceptor symmetry enjoyed in pure H_2O. As a result, they effectively pin down the intrinsic hydrogen bond fluctuation of H_2O. Hence it is also interpreted that the bend, point X, in the Fig. I-7 corresponds to the onset of the crossover to Mixing Scheme II, with Y the end of the process. Namely at this mole fraction $x_{Gly} = 0.16$ at point Y, there are not enough bulk H_2O left to form the percolated hydrogen bond network, and further incoming Gly molecules are forced to aggregates to form Gly-rich clusters in Mixing Scheme II.[22][23]

(6) Various Third Derivatives in Tetrahydrofuran Aqueous Solution

The previous studies mostly treated mono-ols and poly-ols as solute. Here, in order to expand the application of the present differential approach, tetrahydrofuran (THF) is chosen as a new solute. THF has a cyclic ether, of –O– type, whose effect on various third derivative quantities in its aqueous solution are sought. It is well known that the clathrate hydrates, $THF(H_2O)_{17}$, is formed at $x_{THF} = 0.056$ (= 1/(17+1)) and at a temperature lower than 4.5 ˚C.[24] Such information might help in studying the mixing scheme in the aqueous solution. In order to study the mixing schemes further, the various third derivatives of tetrahydrofuran aqueous solution, $V^{E}_{THF\text{-}THF}$, $H^{E}_{THF\text{-}THF}$, $TS^{E}_{THF\text{-}THF}$ and ${}^{SV}\delta_{THF}$, were obtained at 25 ˚C.

(7) Temperature Dependences of Third Derivatives

As stated above, at 25 ˚C the anomalies in various third derivatives of 2-butoxyethanol aqueous solution appear at the same mole fraction. Even at other temperatures, this agreement is conserved. The relationship between the mole fraction and the temperature is shown in Fig. I-13 for $H^{E}_{BE\text{-}BE}$, $TS^{E}_{BE\text{-}BE}$ [25], $V^{E}_{BE\text{-}BE}$[26] and ${}^{SV}\delta_{BE}$ [15]. As evident in the figure, the loci of anomalies for different third derivatives form a single curve that is called as the "Koga line". However, the loci of third derivatives are obtained by graphical differentiation of second or even first derivatives. This operation inevitably increases errors. Therefore, a direct measurement of third derivative, ${}^{SV}\delta_{B}$, was carried out at various temperatures.

Since the direct measurement of ${}^{SV}\delta_{B}$ is expected to provide better data, it is particularly useful for aqueous poly-ols that have small variation in the third derivatives and obscure bend-type anomalous points. Thus, ${}^{SV}\delta_{B}$ measurement for glycerol aqueous solution was carried out for various temperatures in this thesis.

(8) Study of Aqueous Solutions with Other Techniques

Studies on aqueous solutions have been extensively continued by various experimental methods. There is a comprehensive treatise on H_2O and aqueous solutions up to 1980's [29]. However, almost all of these studies did not realize that there are three distinct concentration regions in each

of which the thermodynamic behavior, and hence the mixing scheme, is qualitatively different from that in the other region. Recently, there appear a number of studies hinting such distinction. Sato and Buchner [30] studied aqueous methanol, ethanol, 1-propanol and 2-propanol by dielectric relaxation spectroscopy. They concluded that in the alcohol-rich region, x_{AL} (mole fraction of alcohol) > 0.5, roughly corresponding to Mixing Scheme III, alcohol molecules form clusters by hydrogen bonding among them, to which H_2O molecules are inserted. This scenario is consistent with Mixing Scheme III described above. They take derivative of the activation energy of the relaxation process with respect to x_{AL} and obtained "the excess partial molar activation enthalpy". The latter showed two sharp peaks, the mole fraction loci of which almost coincide with those of point X and Y of the crossover from Mixing Scheme I to II for each alcohol solutions. This hints the presence of the change in mixing scheme in the H_2O-rich region.

Dixit et al. used high resolution Raman spectroscopy to study methanol (ME)-H_2O.[31] From the mole-fraction-dependence of the wave numbers of C–O and C–H stretching modes, they suggested that there are three composition regions each with a distinct structure of methanol and hydration takes place at the chain ends, –OH group. In the intermediate region, $0.2 < x_{ME} < 0.7$, H_2O breaks up methanol chains and methanol molecules also become hydrated individually. By about $x_{ME} \approx 0.15$, –OH groups of methanol are surrounded completely by H_2O and the hydration of $-CH_3$ takes place. At about $x_{ME} \approx 0.05$, the hydration of methanol at $-CH_3$ as well as the –OH

parts is complete. This interpretation is almost completely consistent with Mixing Schemes, III, II, and I, from the methanol-rich end.

A more recent study in 2014 on aqueous methanol, ethanol, 1-propanol and 2-propanol by terahertz time-domain spectroscopy and pulsed field gradient NMR [33] realized that there are three mole fractions that almost coincide with point X, Y and the crossover from Mixing Scheme II to III. In the region below the first mole fraction, a single alcohol molecule is surrounded by H_2O corresponding to Mixing Scheme I. While their analysis contains an ideal mixture assumption in terms of volume fraction without taking partial molar volume in consideration, yet the boundary of Mixing Schemes are similar to those Mixing Scheme I, II, and III.

There has been a long debate about the hydrophobic hydration. In 1945, Frank and Evance suggested the so-called “ice-berg formation”, which dominated the discussions up to about 1990.[32] In more recent years, however, using various spectroscopic technique, the “ice-berg” concept has been contested sharply. Although the existence of the hydration shell around the hydrophobic moiety was supported by these studies, they all deny the ice-like organization within the hydration shell. [33][34][35][36][37]

Koga et al. argued that the increase of the hydrogen bond probability within the hydration shell is offset by the decrease in the hydrogen bond probability of bulk H_2O away from hydration shells.[18] More recently there are MD simulation studies indicating an ordered hydration shells

around CH_4 [38], cyclohexane and benzene in aqueous solutions.[39] [40].

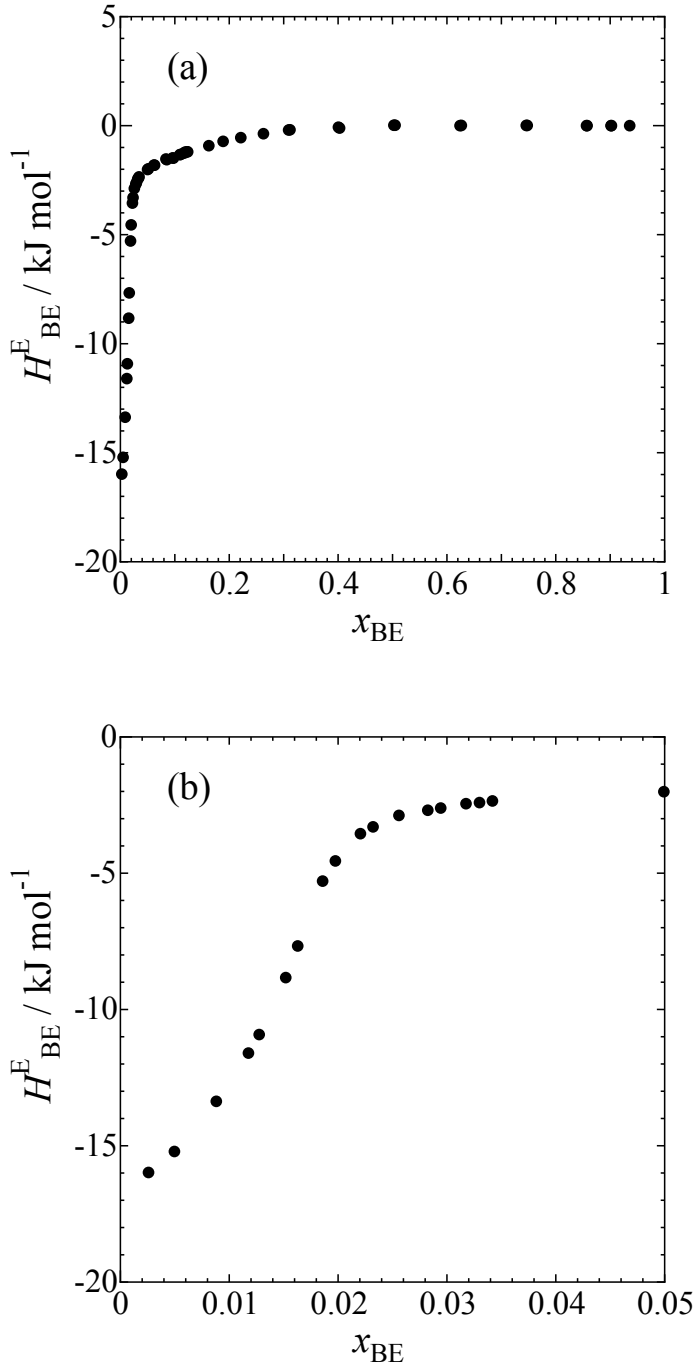

Fig. I-1. The mole-fraction dependences of H^E_{BE} for 2-butoxyethanol aqueous solution at 25 ˚C for all region (a) and dilute region (b).[11]

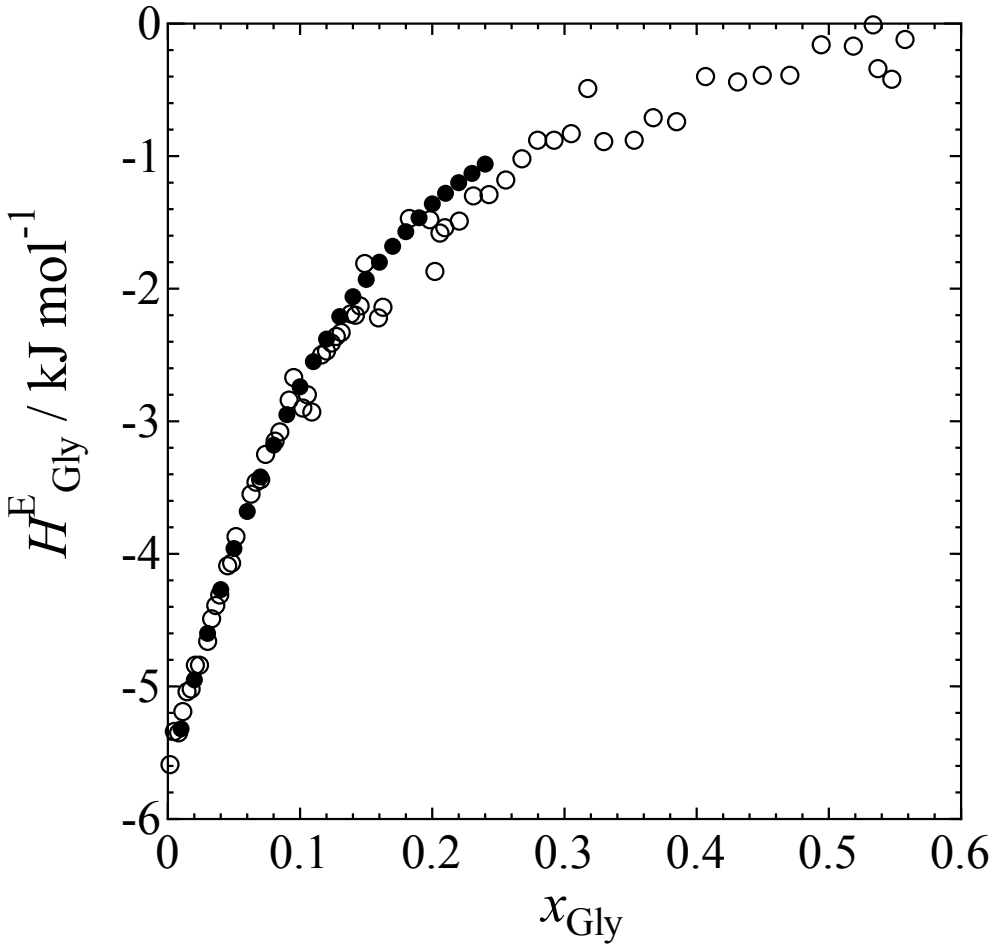

Fig. I-2. The mole-fraction dependences of H^{E}_{Gly} for glycerol aqueous solution at 25 ˚C in filled circle [12] and open circle [13].

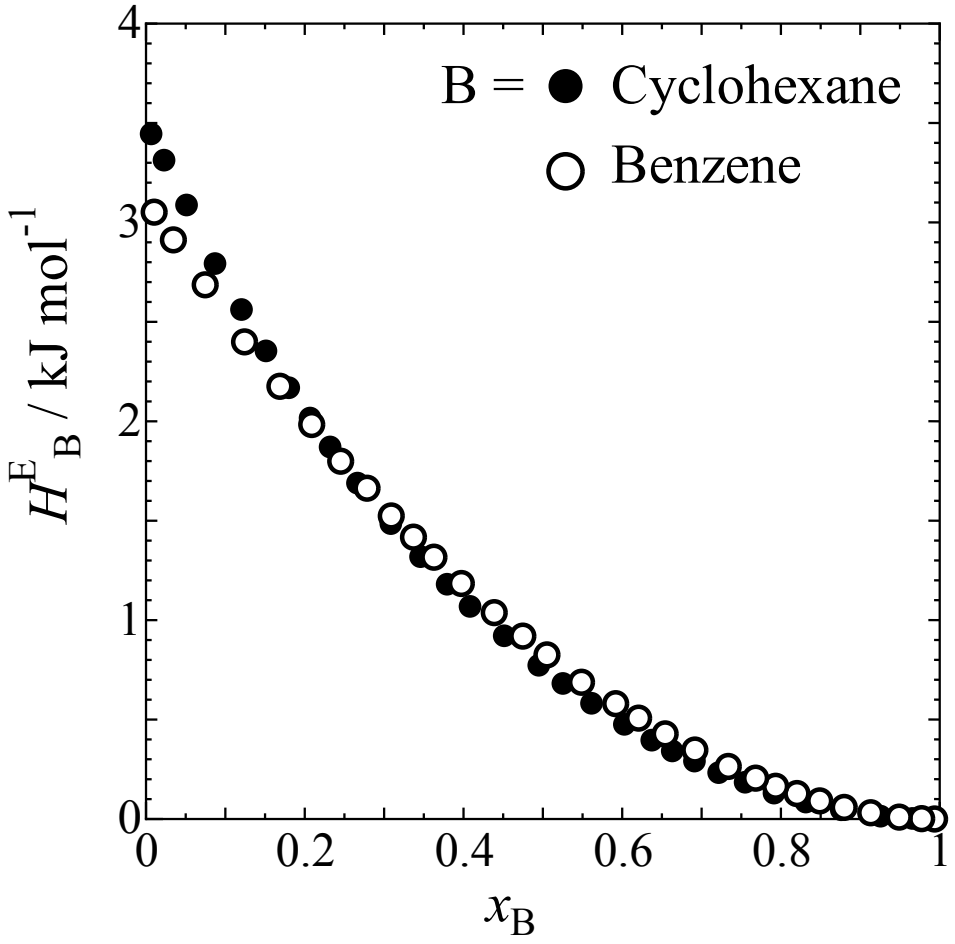

Fig. I-3. The mole-fraction dependences of H^E_B for clyclohexane-benzen solution at 25 ˚C.[14]

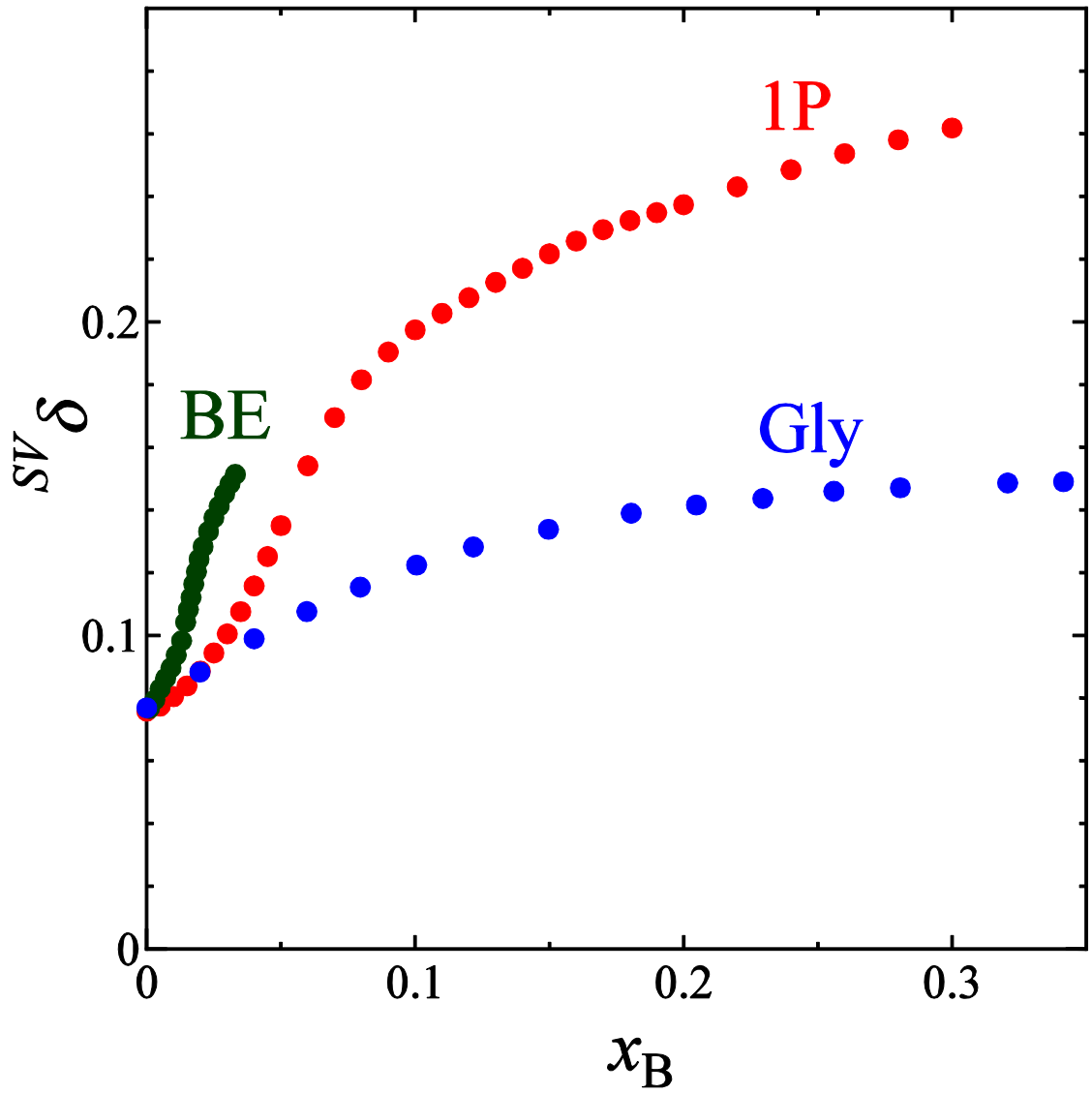

Fig. I-4.The mole fraction dependence of $^{SV}\delta$ for BE, 1P, and Gly aqueous solutions at 25˚C. The Green points are $^{SV}\delta$ of BE aqueous solution, red 1P, and blue Gly. They were calculated from α_p obtained by density. [15][16][13]

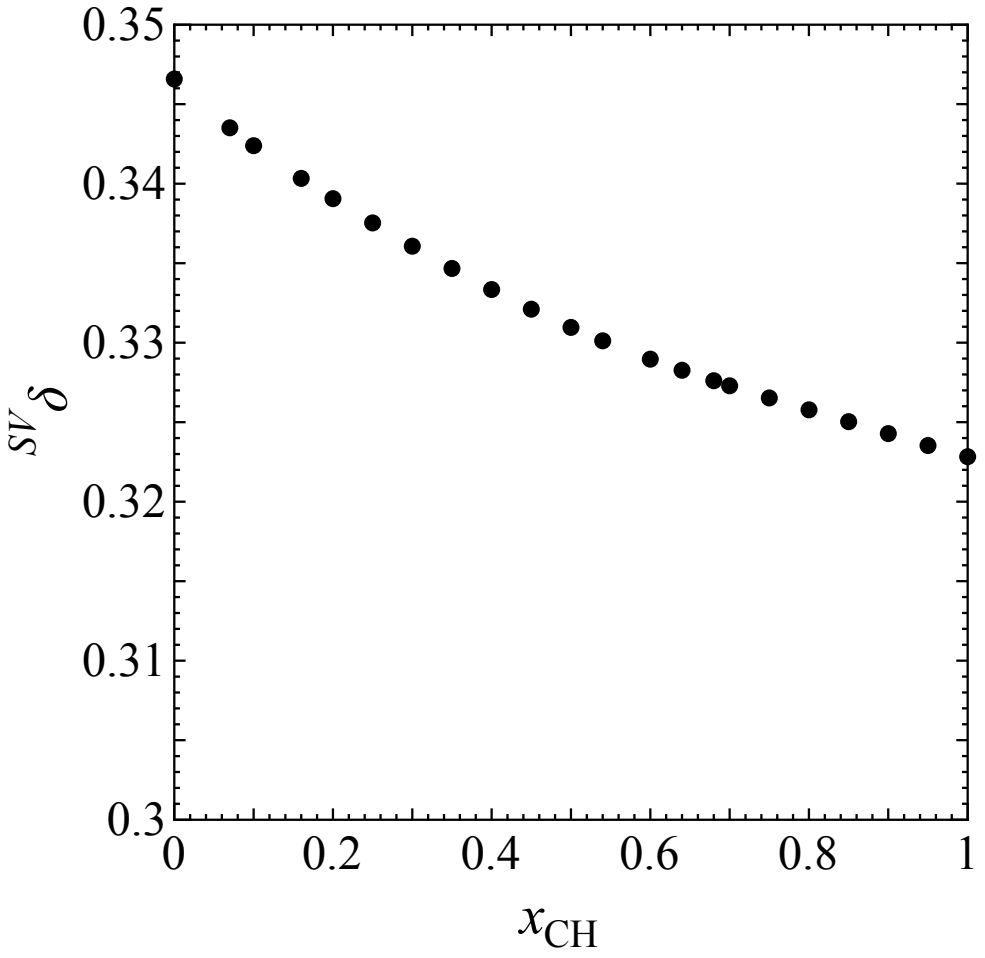

Fig. I-5. The mole fraction dependence of $^{SV}\delta$ in cyclohexane-benzene mixture at 25˚C. $^{SV}\delta$ was calculated from V^E [17].

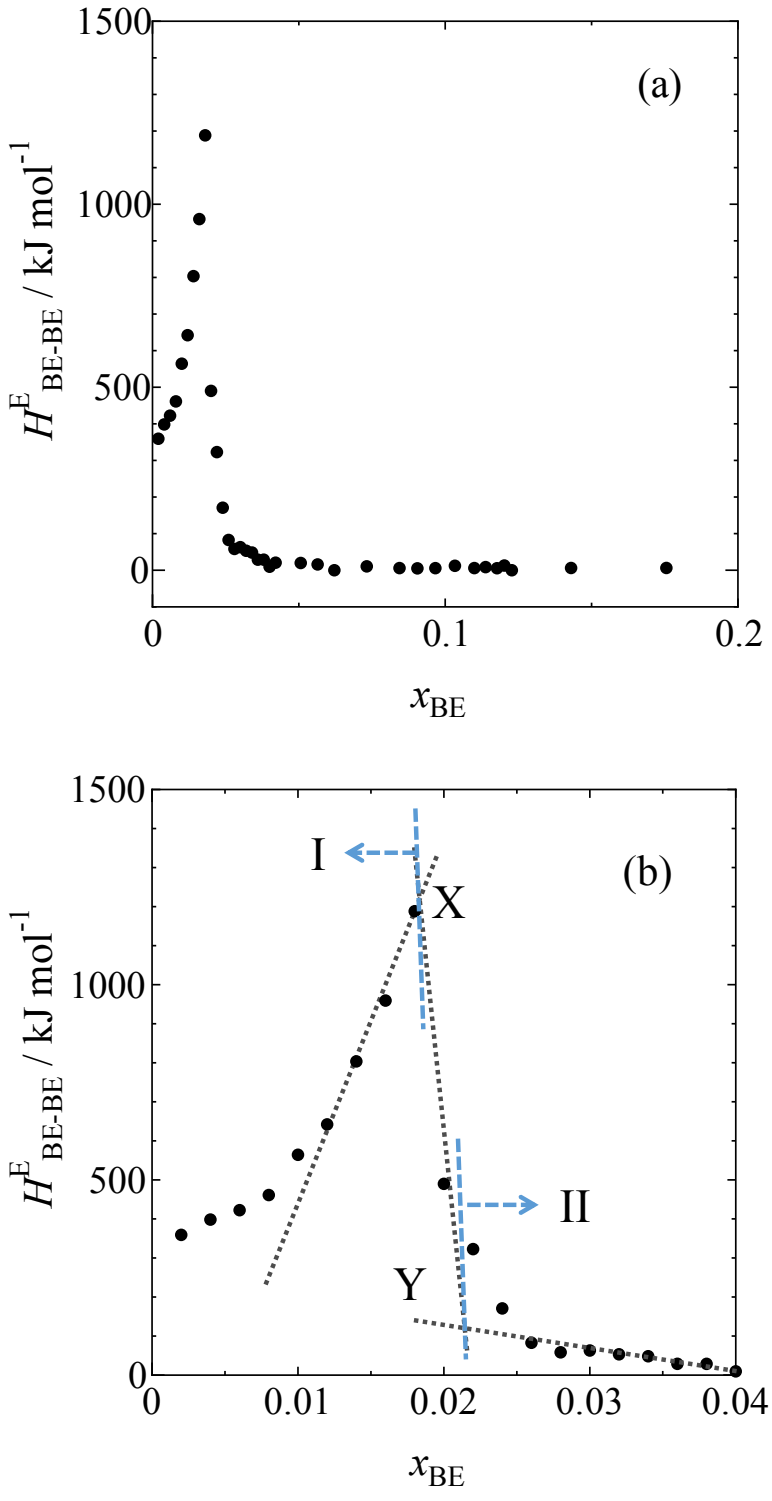

Fig. I-6. The mole fraction dependence of $H^{E}_{BE\text{-}BE}$ for 2-butoxyethanol aqueous solution for all region (a) and dilute region (b).

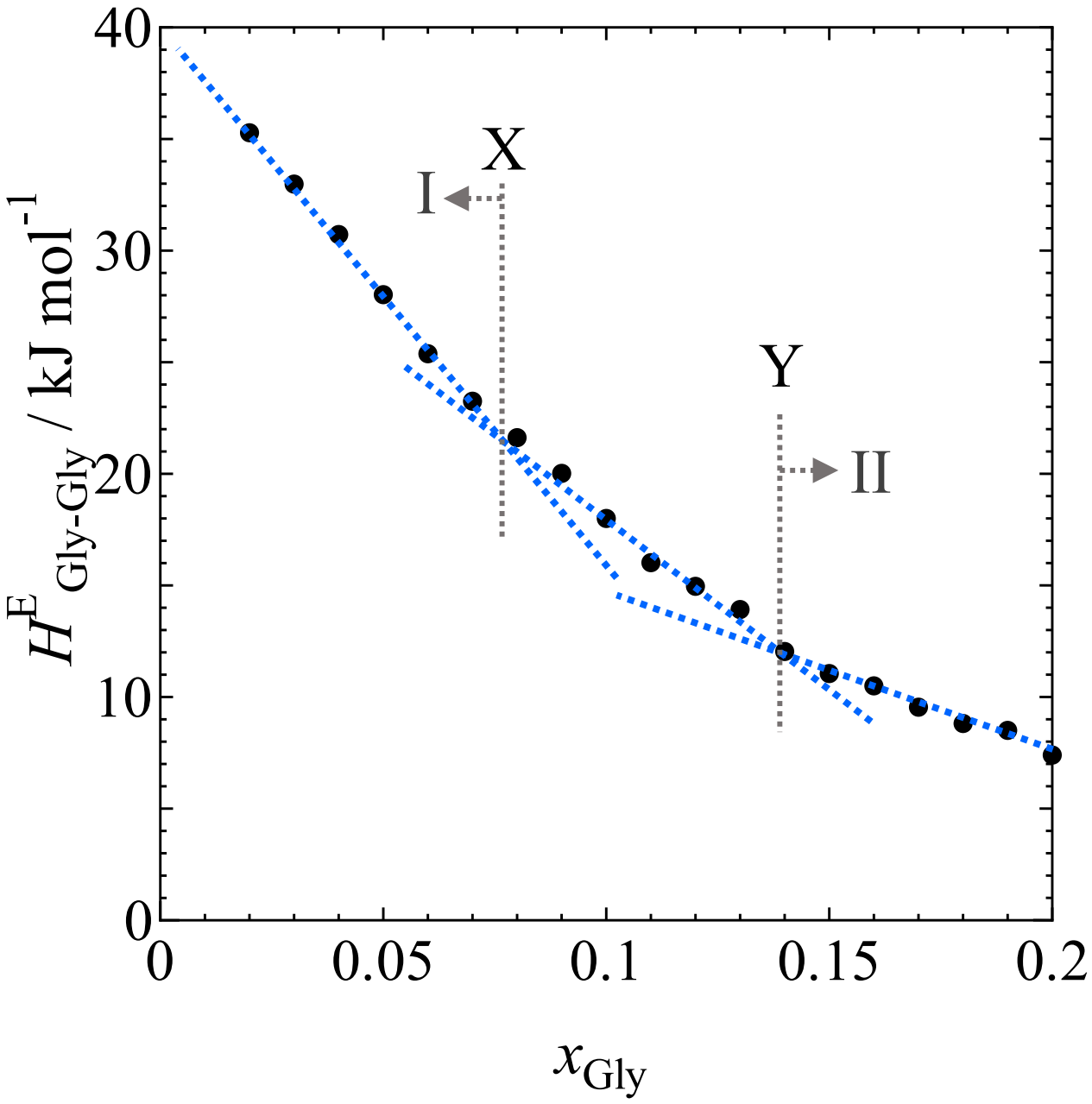

Fig. I-7. The mole-fraction of $H^{E}_{Gly\text{-}Gly}$ of glycerol aqueous solution.

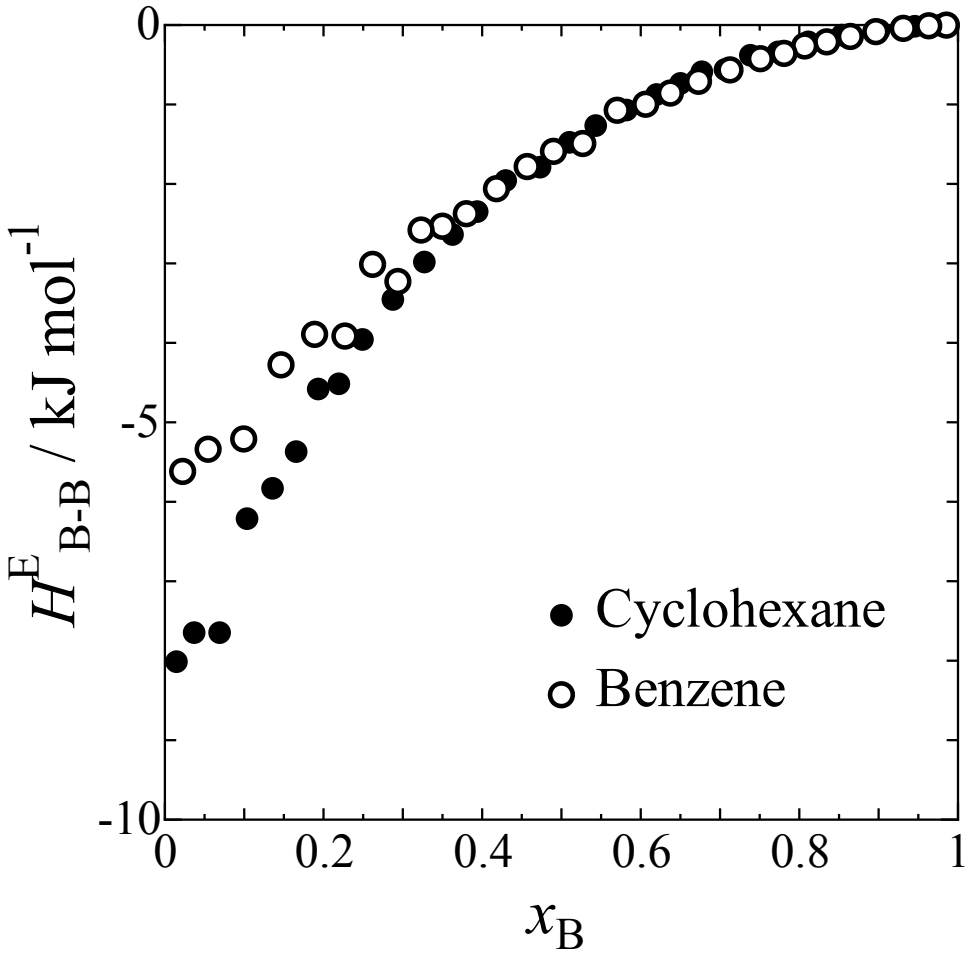

Fig. I-8. The mole fraction dependence of $H^{E}_{B\text{-}B}$ in cyclohexane-benzene mixture.

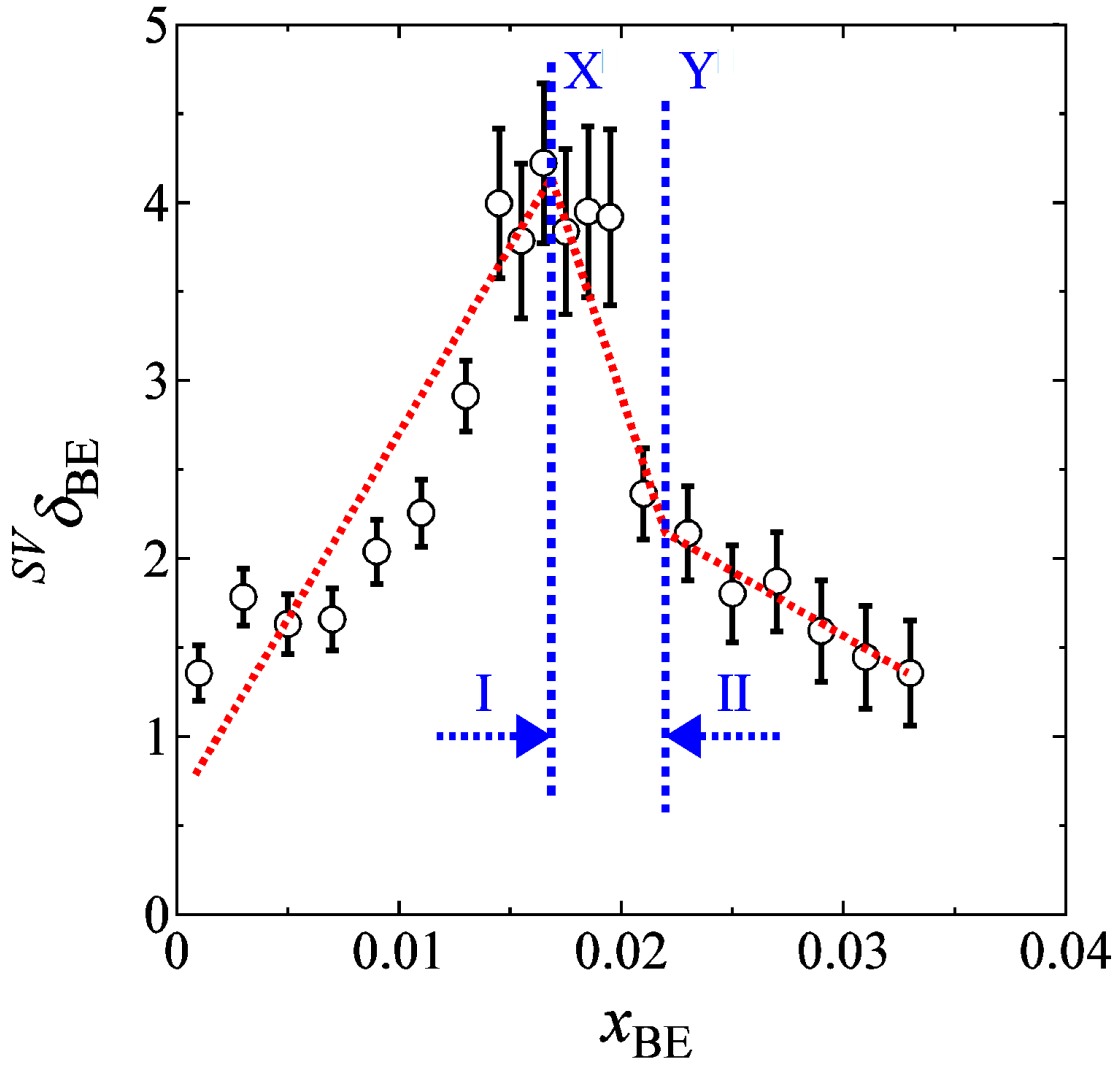

Fig. I-9. The $^{SV}\delta_{BE}$ obtained by graphical differentiation of $^{SV}\delta$ for BE aqueous solution at 25˚C. Points X and Y correspond to the end of Mixing Scheme I and beginning of Mixing Scheme II, respectively.

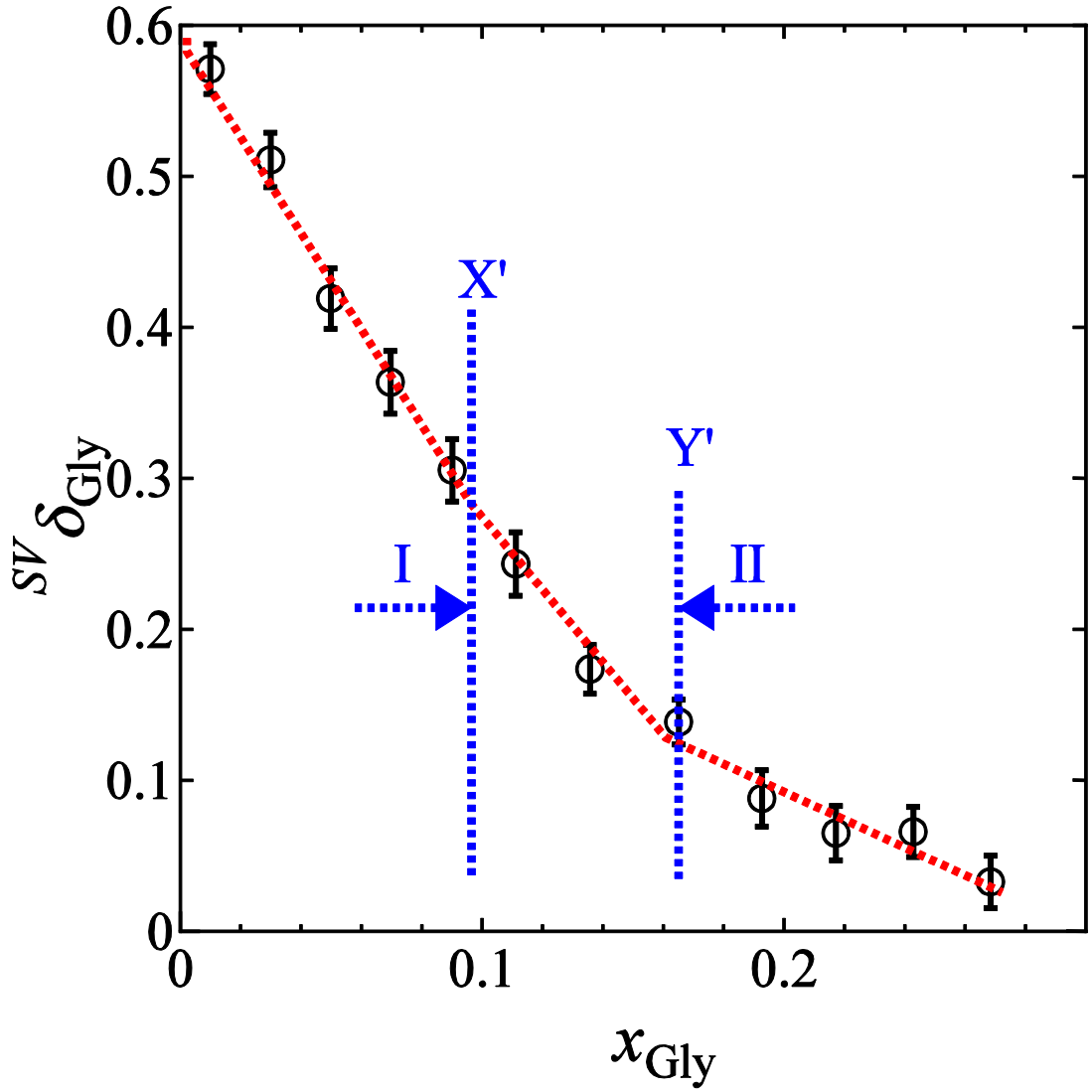

Fig. I-10. The $^{SV}\delta_{Gly}$ obtained by graphical differentiation of $^{SV}\delta$ for Gly aqueous solution at 25˚C.

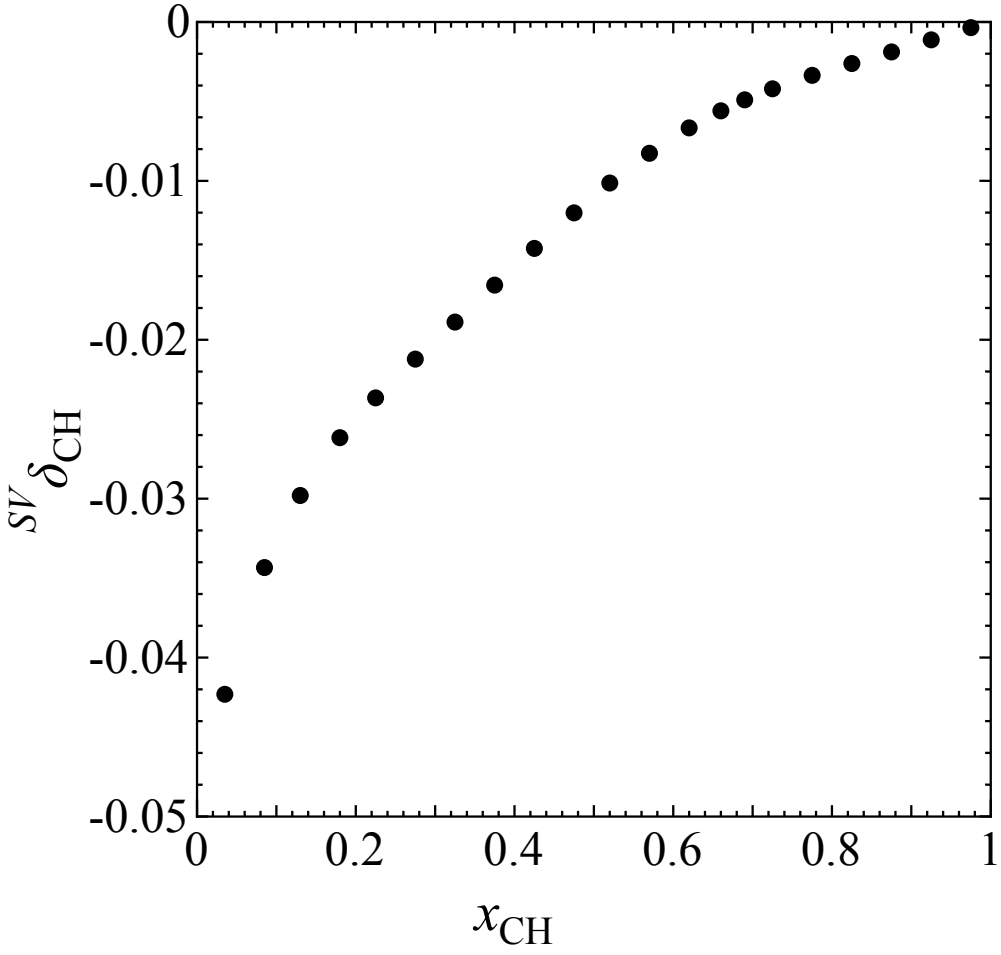

Fig. I-11. The mole fraction dependence of $^{SV}\delta_{CH}$ in cyclohexane-benzene mixture.

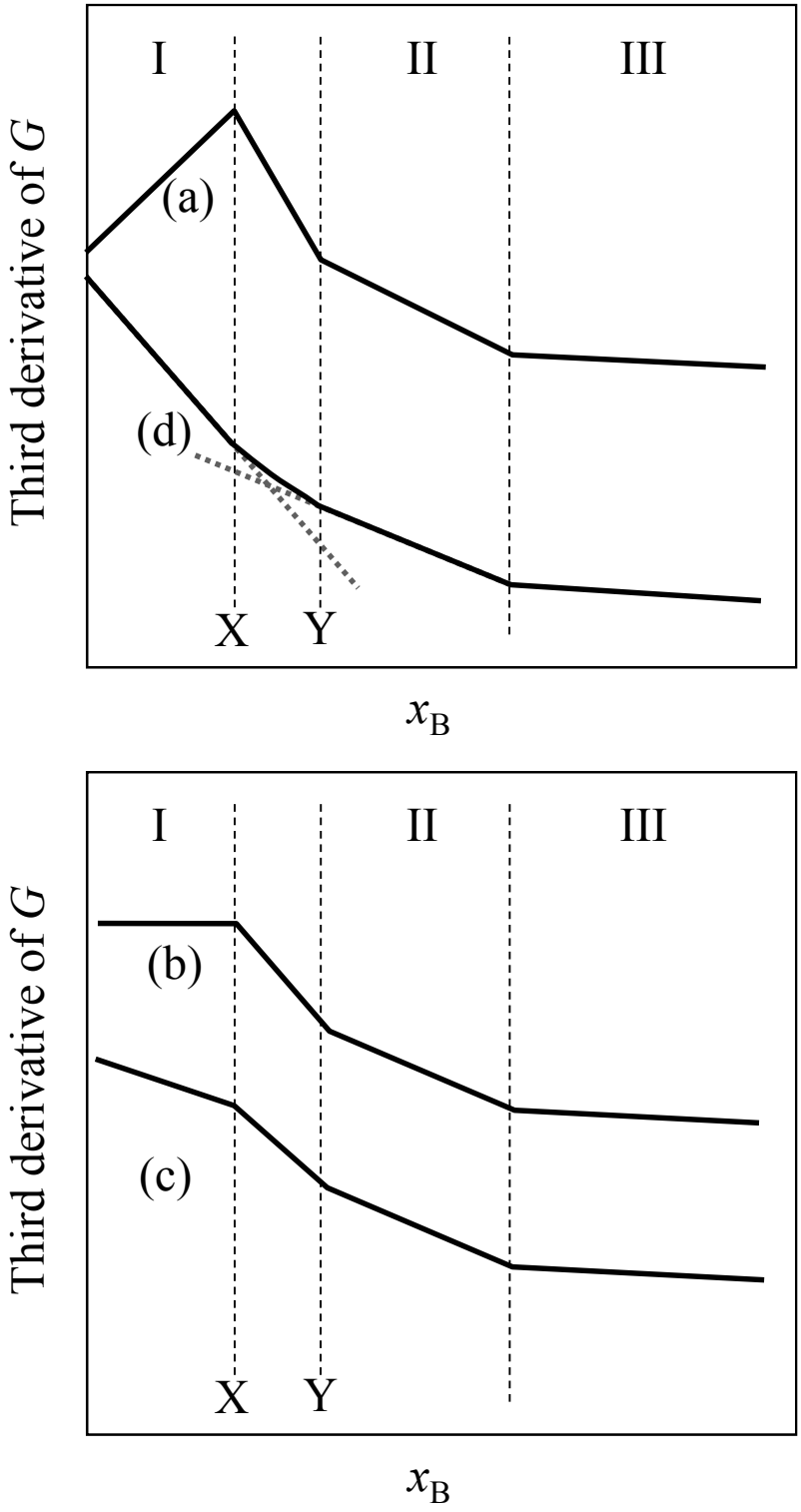

Fig. I-12. The typical mole fraction dependence patterns of third derivatives in aqueous solutions for hydrophobic (a), hydrophilic (d), amphiphilic solute (b, c). The ordinate scale is arbitrary. That for the abscissa is scaled so that anomalies coincide with each other among different kinds of solutes for clarity.

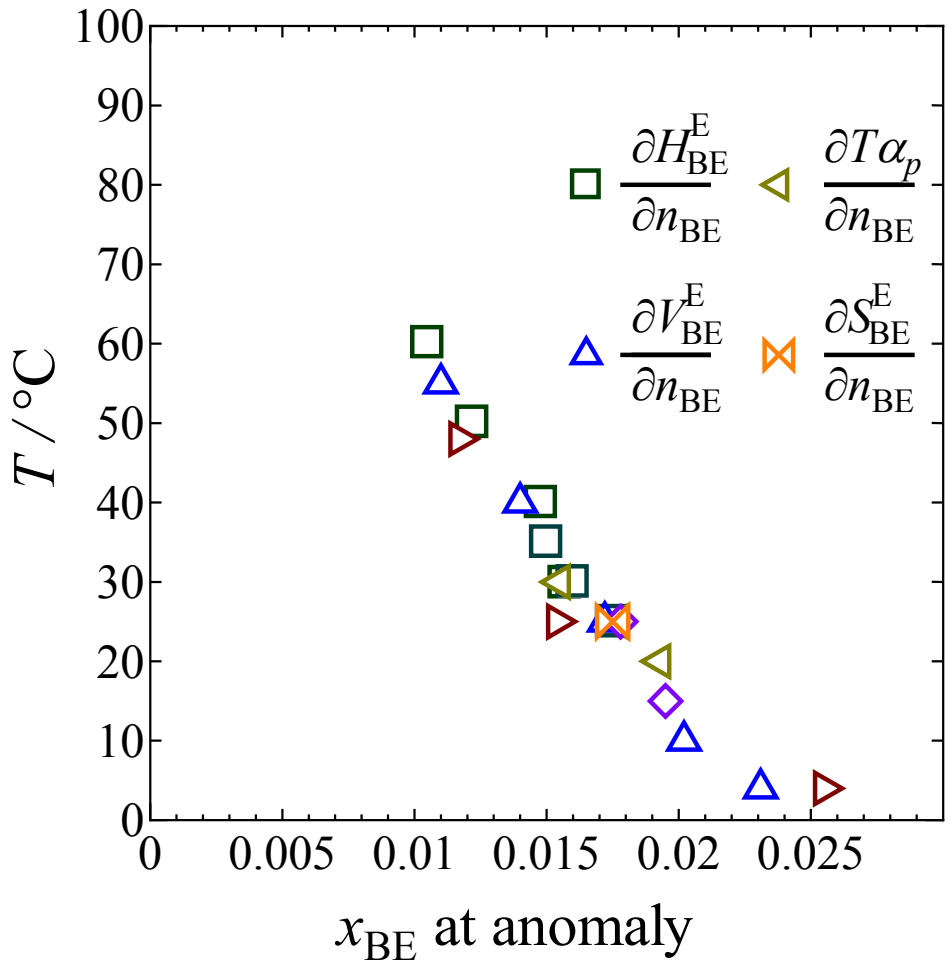

Fig. I-13.The plot of temperature vs. mole fraction at the peak of anomalies for third derivatives, $H^{E}_{BE\text{-}BE}$ [25], $V^{E}_{BE\text{-}BE}$[26], ${}^{SV}\delta_{BE}$ [15] and $TS^{E}_{BE\text{-}BE}$ [25], for 2-bytoxyethanol aqueous solution.

II. Experimental

(1) Samples

Tetrahydrofuran (Sigma-Aldrich, >99.7%), 2-budoxyethanol and glycerol (Wako, special grade) were used as supplied. H_2O with 18.2 MOhm cm^{-1} was taken from a milli-Q water system.

(2) ${}^{SV}\delta_B$ Measurement

In order to experimentally determine a third derivative quantity, a differential pressure perturbation calorimeter was designed and constructed. [28] The design principle is based on the following equation,

$$\alpha_p = \frac{1}{V}\left(\frac{\partial V}{\partial T}\right)_{p,\, n_B} = -\frac{1}{V}\left(\frac{\partial S}{\partial p}\right)_{T,\, n_B} . \tag{16}$$

In this transformation, Maxwell's relation $\left(\frac{\partial V}{\partial T}\right)_{p,\, n_B} = -\left(\frac{\partial S}{\partial p}\right)_{T,\, n_B}$ is used. From thermodynamics definition, $dS = \frac{\delta q_{rev}}{T}$, where δx means a finite but small variation of a quantity x, and q_{rev} is the reversible heat. Then, Eq. (16) can be transformed to be rewritten for a sufficiently small δp as

$$\alpha_p = -\frac{1}{TV}\frac{\delta q}{\delta p} . \tag{17}$$

where subscript "rev" is omitted for brevity. Substituting Eq. (17) into Eq. (14), ${}^{SV}\delta$ can be written as

$${}^{SV}\delta = T\alpha_p = -\frac{1}{V}\frac{\delta q}{\delta p} . \tag{18}$$

Since ${}^{SV}\delta$ is a second derivative, the both side of Eq. (18) are differentiated further with respect to n_B to obtain a third derivative, ${}^{SV}\delta_B$. Using Eq. (15), ${}^{SV}\delta_B$ is

$$ {}^{SV}\delta_B = (1 - x_B) \frac{\partial {}^{SV}\delta_B}{\partial x_B} = -(1 - x_B) \frac{1}{V} \frac{\partial}{\partial x_B} \left(\frac{\delta q}{\delta p} \right), \tag{19} $$

Thus, ${}^{SV}\delta_B$ is obtained by the difference of heats of compression between two samples with slightly different mole fractions.

To experimentally measure ${}^{SV}\delta_B$, an apparatus was fabricated. The outline of this apparatus is described as follows. Identical two cells are prepared. The two cells contain solutions of different mole fractions by Δx_B. Here Δ signifies a small difference between the two cells. By increasing or decreasing pressure by δp to the both samples simultaneously, heats of compression, δq and $\delta(q + \Delta q)$, evolve in the two cells. δ signifies small difference caused by the pressure perturbation. The difference of heat between the two cells, $\delta(\Delta q)$, can be measured by a thermo-module. The voltage of thermo-module, Q_{TM}, is considered to be proportional to Δq, i.e. $\Delta q = kQ_{TM}$, where k is a proportionality apparatus constant containing the heat capacity of the cell assembly and Seebeck coefficient of the thermo-module. Therefore, the difference of ${}^{SV}\delta$, $\Delta^{SV}\delta$, is

$$ \Delta^{SV}\delta = -\frac{k}{V} \frac{\delta Q_{TM}}{\delta p} . \tag{20} $$

${}^{SV}\delta_B$ can be obtained by dividing both sides of Eq. (20) by Δx_B and multiplying by $(1 - x_B)$ following Eq. (15),

$$ {}^{SV}\delta_B = -(1 - x_B) \frac{\Delta}{\Delta x_B} \left(\frac{k}{V} \frac{\delta Q_{TM}}{\delta p} \right) . \tag{21} $$

According to this outline, an apparatus for direct measurement of ${}^{SV}\delta_B$ was fabricated. The schematic drawing of the apparatus and the photo of the cells are shown in Fig. II-1 and Fig. II-2, respectably. A 1 m length of 1/16' OD stainless-steel tubing gold-plated was wound 10.5 times around an aluminum bobbin 30 mm OD × 26.4 mm long, which is also gold-plated. The bobbin has a spiral ditch, 2.6 mm deep, which just fits to the tubing. The inner volume of the tubing is about 0.72 cm^3 and the mass of the cell assembly is 42 g. Thermal contact was facilitated by soldering together the tubing and bobbin. The flat faces of both bobbins were polished and glued using Stycast 1266 (an epoxy resin), sandwiching a thermo-module (Ferrotec LTD.9501/071/030) of 22.4 mm × 22.4 mm × 3.18 mm with 71 pairs of Bi–Te elements. A pre-amplifier (× 100) was inserted in order to increase the signal. The twin cell assembly were encased in a stainless-steel vessel immersed in a constant-temperature bath maintained within ±0.01 ˚C. The bath fluid was water for 25˚C, and oil for higher temperatures than 40˚C.

The sample solutions were filled up to the bottom entrances to the union tee and the hydraulic oil of a low viscosity (Daphne 7373, Idemitsu Co. Ltd.) was filled in the valve and up to the top of the union tee. The thermo-module was used as temperature sensor. An assumption is made that the thermo-module signal, Q_{TM}, is proportional to temperature difference of the two cells, the latter being small in the order of 5 x 10^{-5} K.

The hydraulic pressure was applied to the two cells by using oil-filled stainless-steel valve

(Fujikin Inc., US-326PC), the spindle of which is driven by a computer controlled stepping motor (Oriental Motor Corp., ASM98AAEH100). At the inlet of the valve the strain gauge pressure sensor (Nagano Keiki Co., KM 31-584-Q7) was mounted and through the outlet a length of 0.51 mm OD and 0.25 mm ID stainless-steel tubing is connected to the top of union tee. The difference of temperature between two cells, ΔQ_{TM} were transformed to ${}^{SV}\delta_B$ with equation (21). [28]

The pressure was applied between 0.7 MPa and 4 MPa repeatedly. To suppress possible appearance of air bubbles, the lower pressure was set at a higher pressure than that of atmosphere. On applying or releasing pressure, the Q_{TM} and the pressure traces were monitored for 200 sec, as shown in Fig. II-3. δQ_{TM} is the difference between points A and B. The initial increase in each Q_{TM} trace is ignored because it might reflect the difference of thermal conductivity between two cells. The trace was extrapolated to the time at which pressure was changed, and the temperature difference, δQ_{TM}, and pressure difference, δp were determined from point A and B in the figure.

As a preliminarily experiment, the pressure difference, δp, were varied from 1 to 7 MPa and the signal, $\delta Q_{TM}/\delta p$, was observed to be constant, with error bar increasing as δp increases. Thus, the pressure cycle between 0.7 MPa and 4 MPa were chosen.

The design principle discussed above is based on the premise that the volumes of both cells are identical. In the actuality, however, it is very difficult to make the volumes of two cells exactly the same. Thus, a correction for a difference of volume between two cells should be applied.

Suppose one cell has volume, V, with sample whose mole fraction is x_B. And the other has $V + \Delta V$ and $x_B + \Delta x_B$. ${}^{SV}\delta$ for one cell is ${}^{SV}\delta = \frac{1}{V}\delta q / \delta p$, and for the other is ${}^{SV}\delta = \frac{1}{V + \Delta V}\left\{\frac{\delta(q + \Delta q)}{\delta p}\right\}$.

The difference of ${}^{SV}\delta$ between two cells, $\Delta^{SV}\delta$, is

$$\Delta^{SV}\delta = -\frac{k}{V}\frac{\delta Q_{TM}}{\delta p} - \frac{\Delta V}{V}(T\alpha_p + T\Delta\alpha_p). \tag{22}$$

The second term on the right is the correction term and if $\Delta V = 0$ it vanishes. Thus, we can obtain ${}^{SV}\delta_B$ as

$${}^{SV}\delta_B = -(1 - x_B)\frac{1}{\Delta x_B}\left\{\frac{k}{V}\frac{\delta Q_{TM}}{\delta p} + \frac{\Delta V}{V}(T\alpha_p + T\Delta\alpha_p)\right\}. \tag{23}$$

The parameters in Eq. (23), $\frac{k}{V}$ and $\frac{\Delta V}{V}$ must be determined. For this purpose, one of the two cells was used individually. Namely, the cell was filled with the sample whose α_p is known. Pressure was applied only to this cell and $\delta Q_{TM} / \delta p$ was determined. Eq. (23) for a single cell operation should lead to

$$T\alpha_p = -\frac{k}{V}\frac{\delta Q_{TM}}{\delta p}. \tag{24}$$

Hence, the plots of $T\alpha_p$ against $\delta Q_{TM} / \delta p$ should be linear going through the origin with the slope $-(k/V)$. The same measurements were performed using the other cell as well. The plots of $T\alpha_p$ vs. $\delta Q_{TM} / \delta p$ for water, and BE, 1P, and Gly aqueous solution are shown in Fig. II-4. It is evident that the data points converge into a single straight line for both single cells. This suggests that the value of $\frac{\Delta V}{V}$ is sufficiently small. And the slope should yield $-(k/V)$. However, the intercept has a small but finite value. This is interpreted to show the value to $T\alpha_p$ for the cell itself, whose value

was found from the intercept to be 0.0168. This leads to the value of α_p for the cell to be 5.4 x 10^{-5} K^{-1}, within the same order of magnitude for metals. $\frac{\Delta V}{V}$ can be then determined by measurement with the both cells filled with the same samples. Because $\Delta^{SV}\delta$ and $\Delta\alpha_p$ are zero, Eq. (23) can be transformed to

$$-\frac{k}{V}\frac{\delta Q_{TM}}{\delta p} = \frac{\Delta V}{V} T\alpha_p \quad . \tag{25}$$

$\frac{\Delta V}{V}$ was found to be 0.00011, using water and various BE aqueous solution at 25˚C.

(3) Titration Calorimetry

The excess partial molar enthalpy of THF, H^E_{THF} is determined by using a TAM-2277 Thermal Activity Monitor (Thermometric, Jarfalla, Sweden) with 2250 type calorimeters. A 3 μL aliquot of THF is titrated into about a 0.7 mL solutions of THF-H_2O. The heats evolved through this process δq_{mix} were determined accurately. The quotient, $\delta q_{mix} / \delta n_{THF}$ was approximated as the partial derivative $H^E_{THF} \equiv (\partial H^E / \partial n_{THF})$. This ratio of titrant to titrate is small enough for such an approximation as discussed earlier. [41] The uncertainty in H^E_{THF} was estimated at $\pm$0.1 kJ mol^{-1}. This uncertainty is unusually large. This is likely due to the fact that the value of H^E_{THF} is exceptionally large, hence each aliquot had to be reduced to 3 μL. Yet to cover the mole fraction range up to 0.1, a large syringe with a large bore (the total capacity of 1 mL) was required. Consequently, each travel of the stepping motor that deliver a 3 μL aliquot becomes smaller than

usual, and the relative error becomes larger by that much.

(4) Vapor Pressure

The vapor pressure of aqueous THF was measured by a laboratory-made equipment, a schematic diagram of which is shown in Fig. II-5. The equipment is a stainless steel SS316 and Pyrex glass system with 1/4 " diameter tubing, the 0.5 L and 5L vessels, Nupro bellow Valves(SS-4H), and SS316 to Pyrex transition tubes. An oil-diffusion pump (VPC-500, ULVAC Inc.) evacuates the system to 10^{-4} Pa. The vapor pressure was measured by an MKS 220D Barathron differential capacitance manometer (133 kPa full scale). The sensitivity is ± 1 Pa. The liquid mixture in the cell was prepared by quantitatively mixing THF and H_2O using the gas handling manifold and transferring to the cell kept at liquid nitrogen temperature. The cell is then immersed in a 25 °C bath controlled at 25.00 ± 0.01 °C. The vapor pressure over the liquid phase in the cell was determined by the Barathron gauge. From the results of total vapor pressure as a function of the mole fraction, x_{THF}, in the liquid phase, the partial pressures of THF, p_{THF}, were calculated by the Boissonnas' method.[42][43] From the value of p_{THF}, the excess chemical potential of THF, μ^{E}_{THF}, is obtained by the following equation,

$$\mu^{E}_{THF} = RT \ln \frac{p_{THF}}{x_{THF}\, p^{*}_{THF}} \ , \qquad (26)$$

where R is the gas constant and p^*_{THF} is the vapor pressure of pure THF at 25 °C. The value of p^*_{THF} was found 21.675 kPa which compares with 21.600 kPa from ref.[44]. Since $\mu^E_{THF} = H^E_{THF} - TS^E_{THF}$, S^E_{THF} was calculated using the measured values of H^E_{THF}. With the data of S^E_{THF}, $S^E_{THF\text{-}THF}$ was obtained by graphical differentiation.

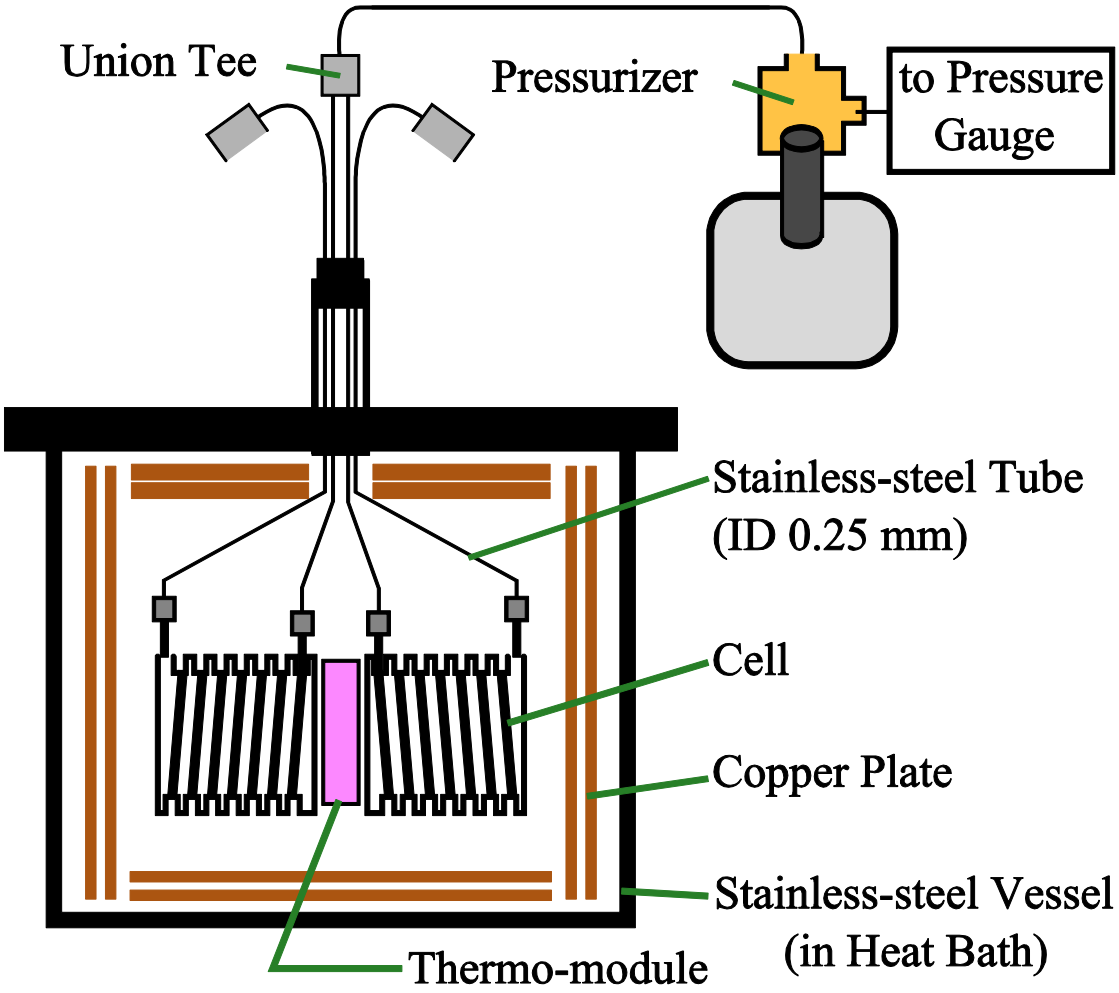

Fig. II-1. Schematic of the home-built apparatus.

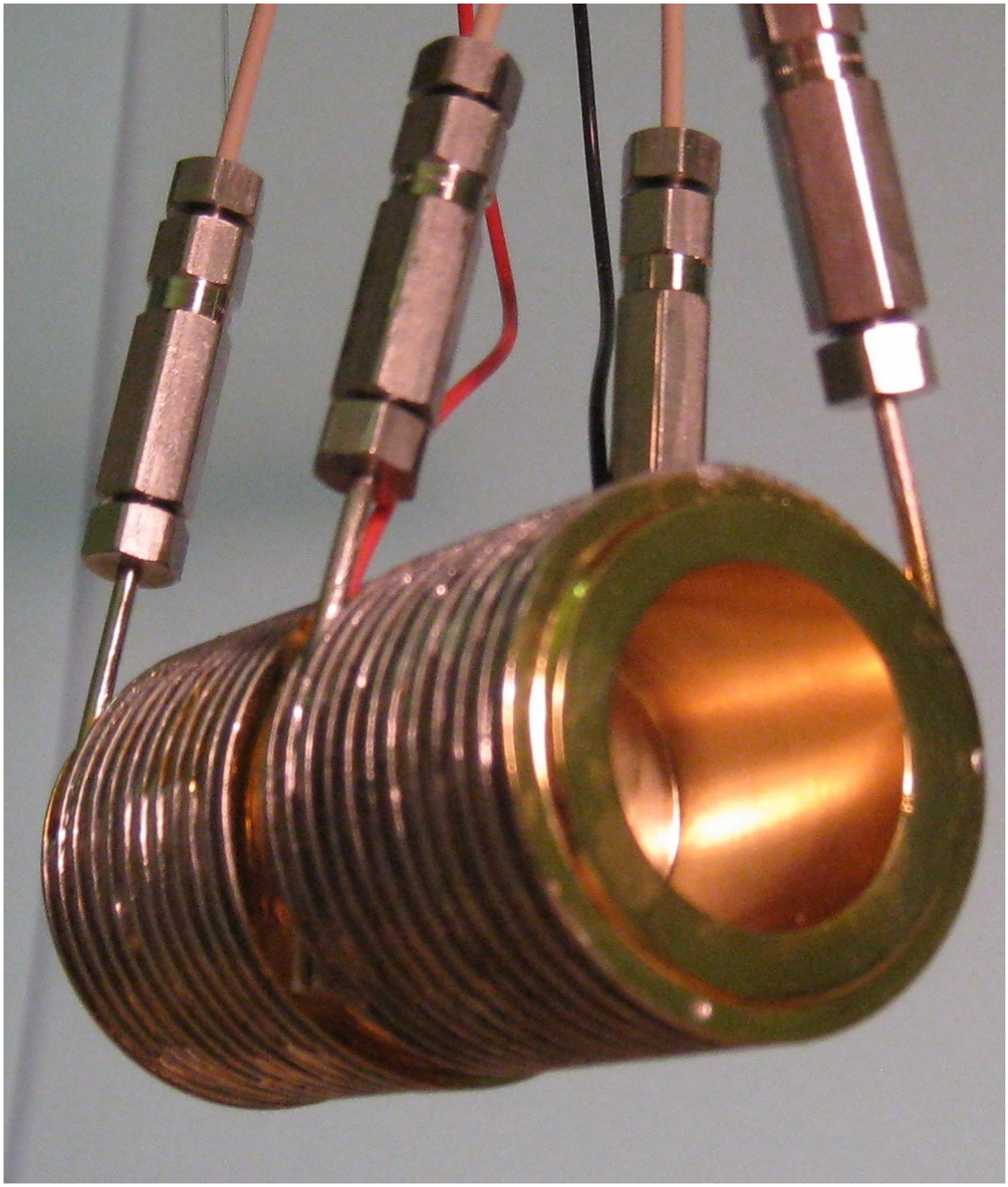

Fig. II-2. Photo of cells.

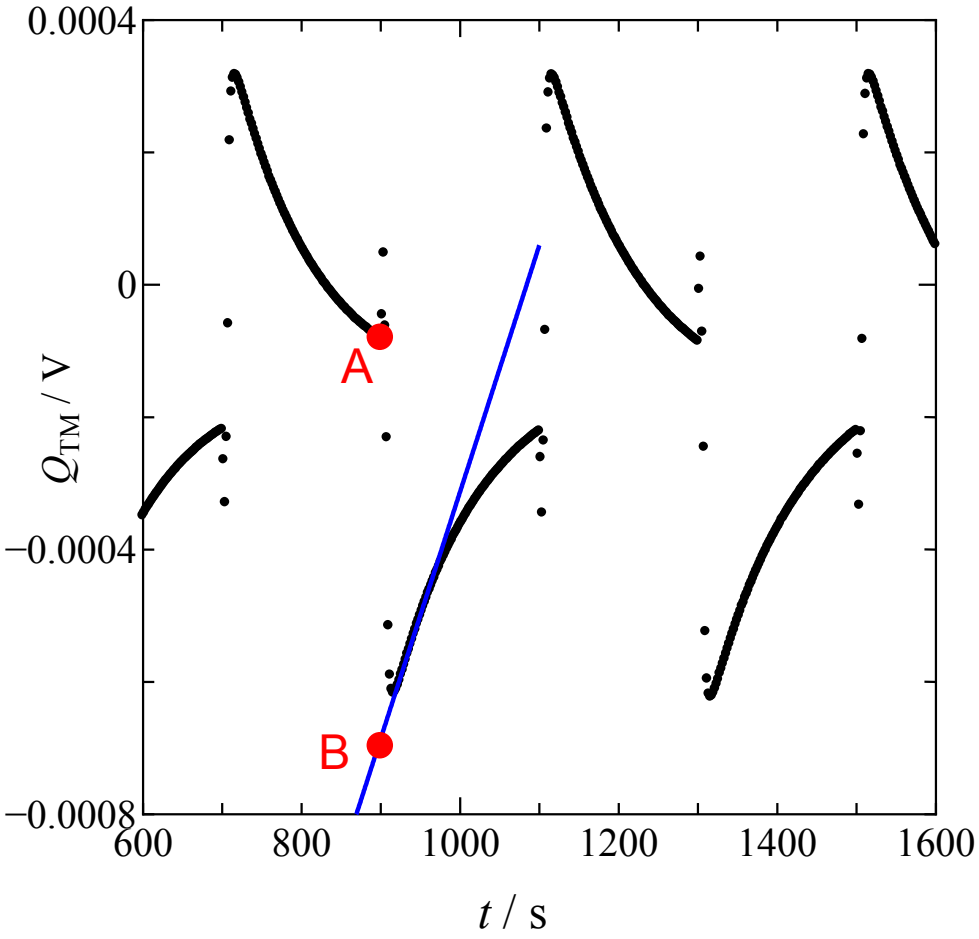

Fig. II-3.The determination of δ Q_{TM} at applying pressure. δ Q_{TM} is the difference between points A and B. The beginning of slope is ignored because it reflected the difference of thermal conductivity between two cells.

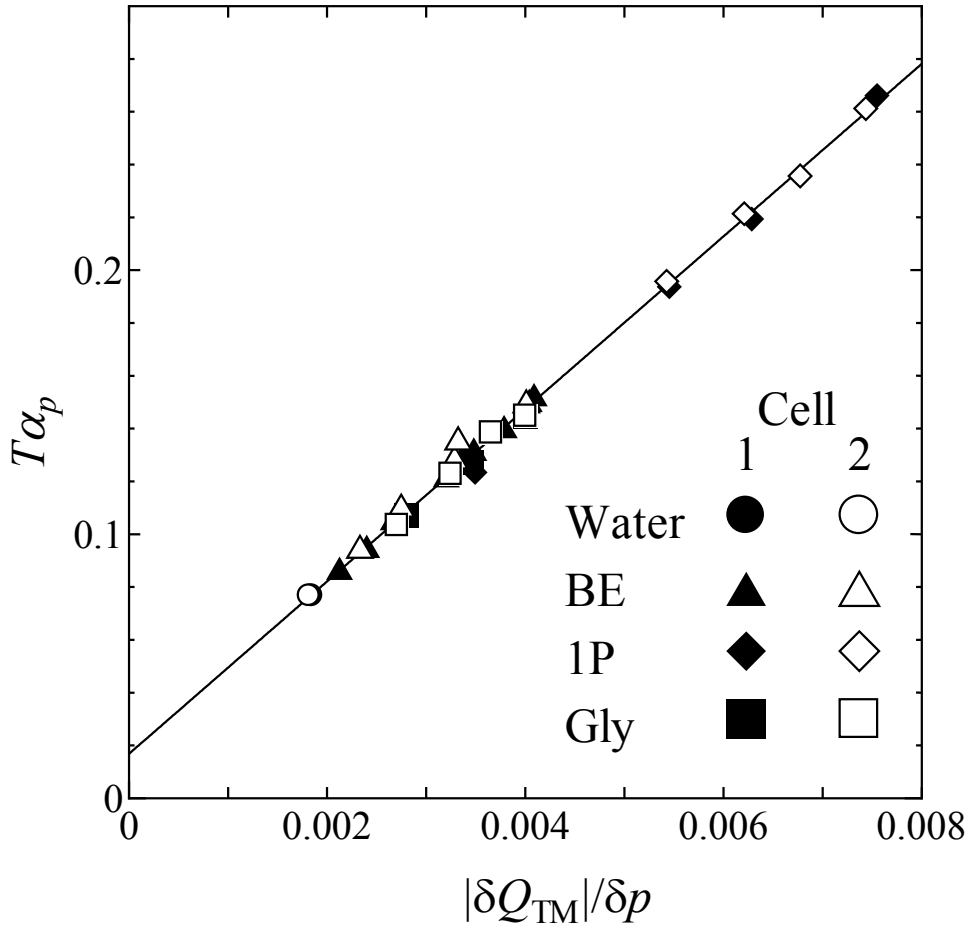

Fig. II-4. Fig. 11. The plots of $T\alpha_p$ vs. $|\delta Q_{TM}| / \delta p$ for water, and 2-butoxyethanol, 1-propanol, and glycerol aqueous solutions in a single cell. Data with cell 1 are filled symbols, those with cell 2 are open symbols. The plots clearly converge into a single straight line. This suggests that $\Delta V/V$ is sufficiently small. See text. The intercept is considered due to an expansion of cell.

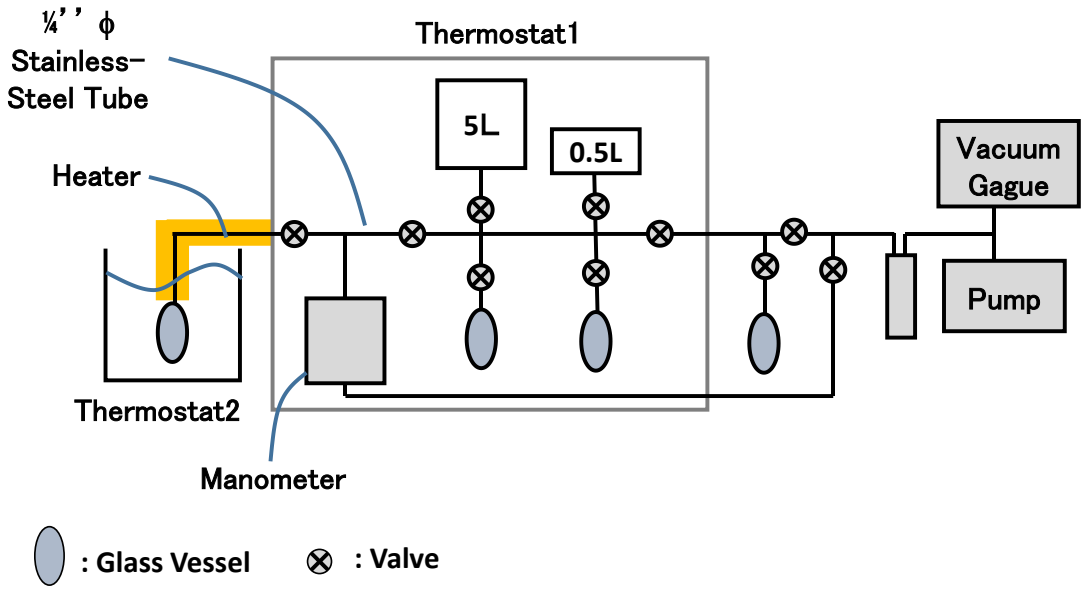

Fig. II-5. The schematic diagram of the equipment to measure vapor pressure. Thermostat 1 and 2 are kept the temperature constant at 40 °C and 25 °C respectively.

III. Results and Discussion

(a) Tetrahydrofuran (THF) Aqueous solution

(a-1) Excess Partial Molar Volume of THF and Volumetric THF-THF Interaction, V^{E}_{THF} and $V^{E}_{THF\text{-}THF}$

First, V^{E}_{THF} was calculated from V^{E} data by Kiyohara et al. [45] by graphical differentiation. The V^{E}_{THF} data are shown in Fig. III-1, together with those for 1-propanol [46] and for glycerol [47]. As is evident in Fig. III-1, below about $x_{THF} = 0.023$, V^{E}_{THF} decreases as mole fraction increases. This initial decrease behavior is also found for aqueous solution of hydrophobic 1-propanol.

Since the values of V^{E}_{THF} were obtained with 3-4 significant digits, we may be able to evaluate $V^{E}_{THF\text{-}THF}$ graphically. A smooth curve was drawn through all the data points of Fig. III-1 and read the values of V^{E}_{THF} off the curve at $\delta x_{THF} = 0.004$ intervals and approximated the partial derivative with the quotient $\delta V^{E}_{THF} / \delta x_{THF}$. The resulting data of $V^{E}_{THF\text{-}THF}$ are shown in Fig. III-2(A). The equivalent quantity of 1-propanol (1P) were calculated by a similar treatment and shown in Fig. III-2(B). Clearly, $V^{E}_{THF\text{-}THF}$ shows a broad peak, much broader than that for 1-propanol. Furthermore, in a more dilute region than the top of the peak, a bend-type anomaly is evident at $x_{THF} = 0.022$. This hints that THF is not simply a hydrophobic solute as 1P.

(a-2) Enthalpic and Entropic THF-THF interactions, $H^{E}_{THF\text{-}THF}$ and $S^{E}_{THF\text{-}THF}$.

The mole-fraction dependences of H^{E}_{THF}, TS^{E}_{THF} and μ^{E}_{THF} are shown in Fig. III-3. The fact that μ^{E}_{THF} is positive indicates the THF-H_2O mixture is unfavorable. This comes from the behavior of H^{E}_{THF} and TS^{E}_{THF}, within the mole fraction range studied, i.e. the THF molecule breaking away from its pure liquid and mix into the solution with a large enthalpy gain of about -13 kJ mol^{-1} with a larger entropy (times T) loss of about -20 kJ mol^{-1} at the infinite dilution. This behavior is similar to the aqueous solutions of mono-ols that were understood to be hydrophobic solutes. Following the principle discussed in Introduction, third derivative quantities, $H^{E}_{THF\text{-}THF}$ and $TS^{E}_{THF\text{-}THF}$, were evaluated graphically. Smooth curves were drawn through all the data points for H^{E}_{THF} and TS^{E}_{THF} as shown in Fig. III-3. Then the data were read off the smooth curves drawn at the x_{THF} interval of 0.004, and the quotients $\delta H^{E}_{THF}/\delta x_{THF}$ were approximated to the partial derivative. The results are shown in Fig. III-4. The top of the peak for $H^{E}_{THF\text{-}THF}$ is at $x_{THF} = 0.022 \pm 0.001$, and that for $TS^{E}_{THF\text{-}THF}$ is at $x_{THF} = 0.022 \pm 0.001$, corresponding to the bend type anomaly of $V^{E}_{THF\text{-}THF}$, Fig. III-2(A). It is noted that point Y is not apparent in Fig. III-4 with the range of measurements.

(a-3) Partial molar entropy-volume cross fluctuation of THF, ${}^{SV}\delta_{THF}$

Fig. III-5 shows the results of ${}^{SV}\delta_{THF}$. The x_{THF}-dependence pattern seems to be similar to that

of $V^{E}_{THF\text{-}THF}$, with the bend anomaly at about $x_{THF} = 0.02$, and the weak peak at $x_{THF} = 0.05$. $H^{E}_{THF\text{-}THF}$ and $TS^{E}_{THF\text{-}THF}$ are the third derivatives of G^{E} with respect to T once and n_{THF} twice; abbreviated as $\{T, n_{THF}, n_{THF}\}$ for convenience. $V^{E}_{THF\text{-}THF}$ is expressed similarly as $\{p, n_{THF}, n_{THF}\}$, and ${}^{SV}\delta_{THF}$ as $\{p, T, n_{THF}\}$. Thus, it can be suggested that the anomalous pattern may depend on the differentiating variables in the present THF-H_2O. It is noted that the latter two third derivatives with similar pattern contain p in the list of the differentiating variables.

(a-4) Similarity to Methanol Aqueous Solution

An attention is now paid into the aqueous solution of the smallest mono-ol, methanol (ME). $H^{E}_{ME\text{-}ME}$ showed a typical peak-type anomaly, though weak, as shown in Fig. III-6 (A), [48] similar to that for $H^{E}_{BE\text{-}BE}$ in Fig. I-6. However, $V^{E}_{ME\text{-}ME}$ in the Fig. III-6(B) calculated from the precise density data [46] shows instead a similar pattern as $V^{E}_{THF\text{-}THF}$, Fig. III-2(A). $V^{E}_{ME\text{-}ME}$ shows a bend type at the same x_{ME} of the peak locus of $H^{E}_{ME\text{-}ME}$ in Fig. III-6(A). Furthermore, the peak top of $V^{E}_{ME\text{-}ME}$ seems to correspond to point Y of $H^{E}_{ME\text{-}ME}$. As shown in Fig. III-2 (B), $V^{E}_{1P\text{-}1P}$ shows a typical peak type anomaly with the bend at the skirt of the peak, which is the correct behavior of hydrophobes. Even for ethanol (ET), $V^{E}_{ET\text{-}ET}$ showed the same pattern as $V^{E}_{1P\text{-}1P}$. After all, methanol has one –OH and one CH_3–, and perhaps it should be regarded more correctly as an amphiphile. Having realized this, we suggest that THF is also an amphiphile. Furthermore, the

mole fraction dependence pattern of the third derivative quantities have been regarded as showing the same pattern for hydrophobes and hydrophiles. The present case indicates that amphiphiles are more complicated in this regard. The third derivative patterns are not necessarily the same among all third derivatives within given amphiphilic solute. Namely, the mole fraction dependence pattern of a third derivative could be related to the variable of differentiation. Here, $H^{E}_{THF\text{-}THF}$ and $H^{E}_{ME\text{-}ME}$ show the peak type first pattern while $V^{E}_{THF\text{-}THF}$, and $V^{E}_{ME\text{-}ME}$ showed the bend first followed by the peak at point Y. For a hydrophobe or hydrophile the mole fraction dependence patterns of the third derivatives were found to be the same for a given solute, as discussed in section I-(4). For amphiphiles, however, the third derivative patterns seem different dependent of the identity of the third derivative. As was observed here, $H^{E}_{THF\text{-}THF}$ pattern and $TS^{E}_{THF\text{-}THF}$ abbreviated as $\{T, n_{THF}, n_{THF}\}$ showed peak at point X. Although point Y is not apparent within the obtained data. $V^{E}_{THF\text{-}THF}$ $\{ p, n_{THF}, n_{THF} \}$ and ${}^{SV}\delta_{THF}$ $\{T, p, n_{THF} \}$, on the other hand, gave a bend anomaly at X followed by a weak peak at Y. Thus, the respective contributions from the hydrophobic and the hydrophilic moieties could tip a balance between the two effects depending on the list of differentiating variables. It is noted that $V^{E}_{THF\text{-}THF}$ and ${}^{SV}\delta_{THF}$ showed the similar patterns and that both contains p as one of differentiating variables. There are countless amphiphiles, and further investigations seem to be necessary to sort the cases for all amphiphiles.

(b) Temperature Dependence of Third Derivatives for Aqueous Solutions of hydrophobe and hydrophile

In this section, the temperature dependences of the third derivative quantities in some aqueous solutions are studied by directly determining ${}^{SV}\delta_{B}$. For the latter measurements a typical hydrohpobe, 2-buoxyethanol (BE), and a hydrophile, glycerol (Gly) are chosen. As will become evident, the anomalous point show the temperature dependence such that its extrapolation to the infinite dilution seems to point universally to about 60-70 ˚C, regardless of the identity of solute. This suggests that for a pure water, there could be a subtle cross over in the molecular organization in pure H_2O at the same temperature.

(b-1) ${}^{SV}\delta_{BE}$ for 2-Butoxyethanol Aqueous Solution

The results of ${}^{SV}\delta_{BE}$ for 2-butoxyethanol aqueous solution are shown in Fig. III-7. Clearly, the peak-type anomaly is apparent at each temperature. This peak-type anomaly indicates that 2-butoxyethanol has hydrophobic nature in aqueous solution. As temperature increases, the mole fraction and the height of peak decrease. Fig. III-8 shows both ${}^{SV}\delta_{BE}$ at 25 ˚C and 40 ˚C. $H^{E}_{BE\text{-}BE}$, another third derivative, is also shown in the figure at the same temperature. Their patterns of the mole-fraction dependence and the values of mole fraction at point X and Y are the same. We interpret from these observations that in the region from the infinite dilution to the top of peak,

point X, Mixing Scheme I is operative, while beyond point Y there exist two kinds of clusters, one rich in H_2O and the other in 2-butoxyethanol molecules, i.e. Mixing Scheme II as discussed above.

(b-2) ${}^{SV}\delta_{Gly}$ for Glycerol Aqueous Solution

The results of ${}^{SV}\delta_{Gly}$ for glycerol aqueous solution are shown in Fig. III-9. In contrast to the 2-butoxyethanol case, ${}^{SV}\delta_{Gly}$ decreases as x_{Gly} increases for each temperature, and it seems there are bend-type anomalies. Namely, there are two straight line branches with a certain transient region in between them. If so, the next derivative should show a step. Fig. III-10 shows the fourth derivative, ${}^{SV}\delta_{Gly\text{-}Gly}$, defined by the following equation. [50]

$$ {}^{SV}\delta_{Gly\text{-}Gly} = N\frac{\partial^{SV}\delta_{Gly}}{\partial n_{Gly}} = (1 - x_{Gly})\frac{\partial^{SV}\delta_{Gly}}{\partial x_{Gly}}. \quad (27) $$

Clearly, there are step type x_{Gly}-dependences. However, the fact that the two straight lines are not flat (constant) but with a slope indicates that the two branches in the third derivative quantity, ${}^{SV}\delta_{Gly}$, Fig. III-9, are not strictly a straight lines, but are slightly curved. Nevertheless, two branches are clearly apparent. Therefore, it is suggested that each branch shows specific characters with the transient region starting at the onset of the step, X, and ending at the end point Y, as shown in the figure. This pattern is specific for solute Gly, i.e. a hydrophilic solute. Namely,

from the infinite dilution to point X is Mixing Scheme I region and in the region beyond point Y Mixing Scheme II is operative.

(b-3) Tempearture Dependence of x_B at the Anomaly.

For both 2-butoxythenoal (BE) and glycerol (Gly), the value of x_B at point X of ${}^{SV}\delta_B$ and that of $H^E_{B\text{-}B}$ decreases as temperature increases. As is clear from Fig. III-8 for BE-H_2O and Fig. III-11 for Gly-H_2O, the x_B-dependence patterns are the same within a given solute. Thus, for hydrophobic as well as hydrophilic solutes, all third derivative quantities seem to take the same pattern regardless of the identity of third derivative (As discussed above for the THF-H_2O case, the third derivative patterns for amphiphiles could take different forms depending on the identity of the third derivative.) Fig. III-12 is the collection of the x_B loci of anomalies for all the hydrophobes and the hydrophile studied so far. In the figure Gly is a hydrophile, but all the other solutes are hydrophobes from previous studies. [25]][27][51] The collection of the anomalies from various types of third derivatives for a given solute seem to form a single curve that is called as the "Koga Line." Namely, there should be as many Koga Lines as the number of solutes. What is striking is that all the Koga lines seem to extrapolate to the infinite dilution, $x_B = 0$, to the unique temperature, 60-70 ˚C independent of the identity of solute. The same is true for a hydrophilic Gly. This suggests that there should be a subtle change in physics of pure liquid water at the same

temperature. The Koga line is the boundary of Mixing Scheme I and II, i.e. the point at which the hydrogen-bond percolation starts to be broken. Thus, the hydrogen-bond percolation of even pure water may be broken at the same temperature, as Stanley and Teixeira suggested. [8]

(b-4) Pressure Derivative of κ_T of Pure Water

In this section, any singularity in third derivative quantities is sought at around 60 to 70 ˚C for pure H_2O. [52] There are a vast amount of thermodynamic data available in literature for H_2O.[53][54][55] However, they are without exception smoothed by analytic functions of various complexity. As pointed out in Introduction, the curve-fitted data tend to mask any singular behavior and any anomalous point in the next derivative would be missed. Therefore very accurate raw data are required at least at the second derivative level, i.e. response functions, in small increments in an independent variable p or T. Fortunately there are speed of sound, u, [56] and specific volume data, v, [57], raw data of which are listed in small enough increments in p at several fixed identical temperatures. From them κ_S can be calculated as,

$$\kappa_S = v/u^2. \tag{28}$$

κ_S is a second derivative quantity. However, we would like to obtain the p-derivative keeping the other independent variable T constant. For this purpose, κ_T data are required. Since κ_T is calculated by,

$$\kappa_T = \kappa_S + Tv\alpha_p^2/c_p, \tag{29}$$

(a_p is specific thermal expansivity, and c_p specific heat capacity), we need good data for α_P and c_p. As will become evident below, the correction term on the right of eq. (29) is at most several percent of the first term. Hence any singular behavior of the second term may be negligible and the literature data, though smoothed, for α_P and c_p [53] are used.

The results are shown in Fig. III-13. As pressure increases, the values of κ_T decrease probably due to reduction of intermolecular distance and free space for fluctuation. (κ_T is related to the volume fluctuation density. [58]) Our purpose is to obtain a third derivative quantity without resorting to any fitting function. Now that κ_T data were obtained as a function of p at a fixed temperature, $\partial\kappa_T / \partial p$, is calculated numerically using two adjacent data points. The resulting third derivative data are shown in Fig. III-14. As pressure increases, $\partial\kappa_T / \partial p$ increases almost linear at low p-region and then starts to deviate at higher p-range. This resembles the bend-type anomaly for ${}^{SV}\delta_{\mathrm{Gly}}$ against x_{Gly} as shown in Fig. III-9, though upside down. To make this anomaly clear, the next x_{Gly} derivative, ${}^{SV}\delta_{\mathrm{Gly\text{-}Gly}}$, was taken as shown in Fig. III-10. [59] The fact that there is a step anomaly in the figure assured the existence of the bend-anomaly in ${}^{SV}\delta_{\mathrm{Gly}}$. Similarly, here one more p-derivative, the fourth derivative, $\partial^2\kappa_T / \partial p^2$ was obtained. The resulting pressure dependence of $\partial^2\kappa_T / \partial p^2$ is shown in Fig. III-15. At low temperatures, step-type anomalies are apparent. The beginning of the step is called as point X and the end as Y as for ${}^{SV}\delta_{\mathrm{Gly\text{-}Gly}}$. At higher

temperatures than 313 K, point X is not clearly defined. They must be at a smaller *p*, less than 30 MPa, if present.

The pressure dependence of point X and Y is shown in Fig. III-16 (open circle). Fig. III-16 also displays the phase diagram of water [60] [61] and a boundary between “high-” and “low-density” liquid from MD simulation [62] and Brillouin scattering [63]. The extrapolation of middle points of point X and Y (red filled circle) to lower temperature points to the triple point of liquid, ice Ih and ice III. Thus, the curve formed by middle points could be related to the boundary between what has been known as the “low density water” and the "high density water". The various blue up triangles in Fig. III-16 were determined by Fanetti et.al using femtosecond pump probe spectroscopy, separating two kinds of water. [64]

Extrapolation of point X from Fig. III-16 to the ordinary pressure (= 0.1 MPa) reaches 60-70 ˚C. This coincides with the temperature obtained by extrapolation of the Koga lines (collection of point X’s) to the infinite dilution at 0.1 MPa. This coincidence suggests that even in pure water the region below this temperature must have the same molecular organization of H_2O as in Mixing Scheme I. Namely the hydrogen bond network is bond-percolated, the extreme case of which is seen in ice Ih. Therefore, the liquid H_2O in this region corresponds to the "low density liquid" and is proposed to be called as "liquid Ih".

In the “high density water” H_2O molecules must effectively fill in gaps in the hydrogen bond network. Therefore, there would be no hydrogen bond percolation is present any longer. Thus, we suggest that at point Y in pure water, hydrogen bond percolation is broken completely, and at point X the percolation begins to be broken.

Stanley and Teixeira [8] advanced the site-correlated percolation model for pure H_2O and they estimated the global hydrogen bond probability as a function of temperature from the density data of H_2O. According to their estimate, the hydrogen bond probability reaches 39 %[9], which is the bond-percolation threshold of ice Ih type bond connectivity, at about 80 ˚C [18]. This temperature is strikingly near the extrapolated temperature of about 60−70 ˚C. Then, it may be appropriate to conclude there is a crossover in the molecular organization in pure H_2O at this temperature at 0.1 MPa.

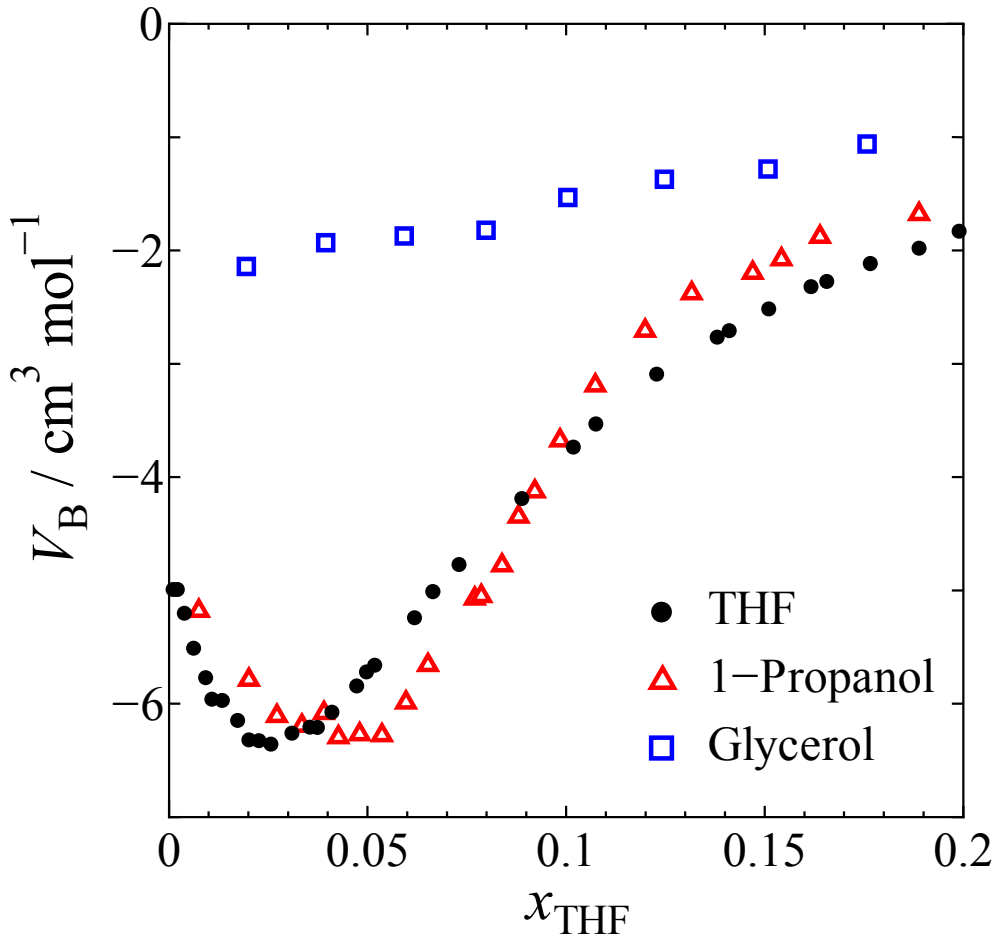

Fig. III-1. The mole-fraction dependence of V^E_B in aqueous solutions of tetrahydrofuran (black circle), 1-propanol (red triangle) and glycerol (blue circle) at 25 ˚C.

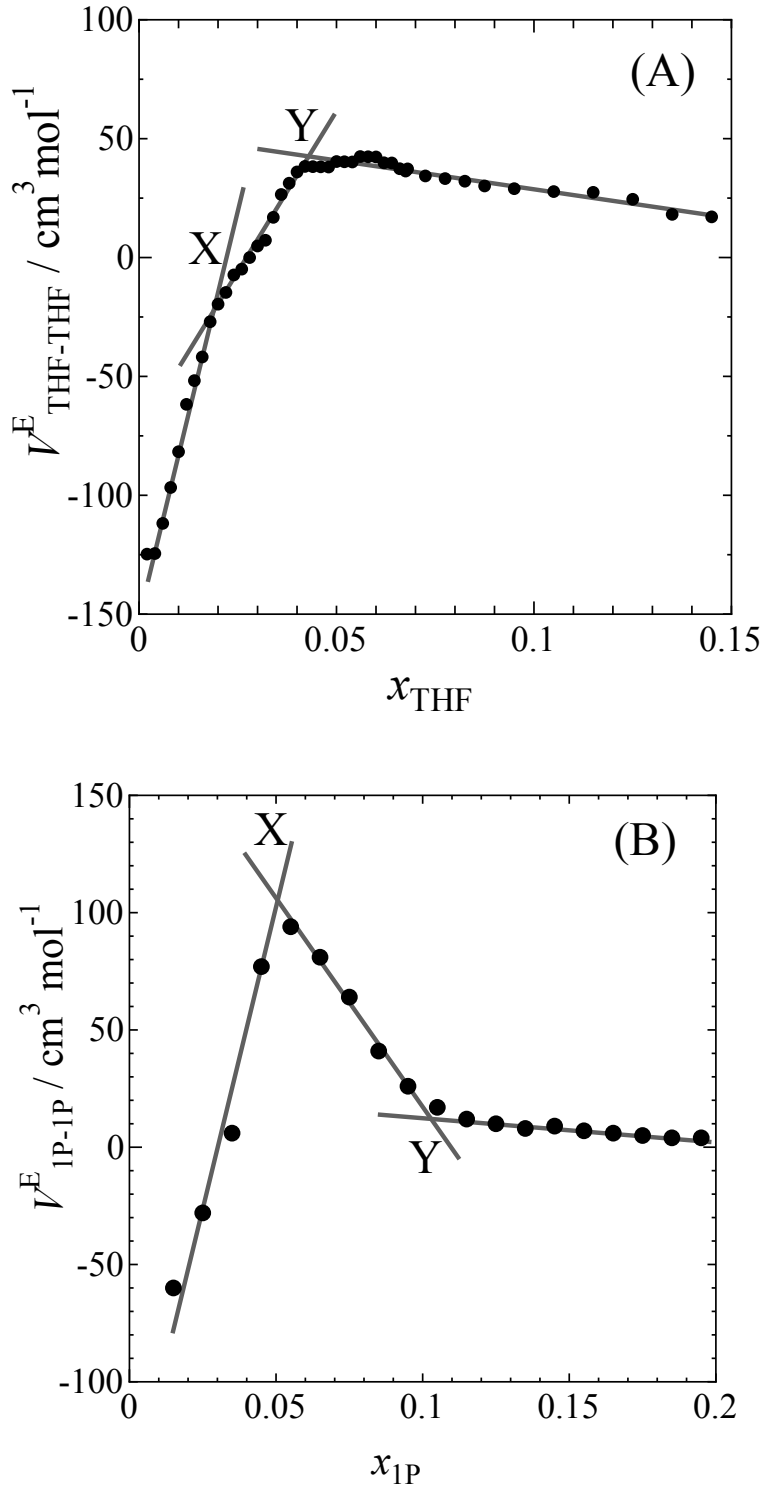

Fig. III-2. The mole-fraction dependence of $V^E_{THF-THF}$ in aqueous THF (A) and $V^E_{THF-THF}$ in aqueous 1P (B) at 25 ˚C.

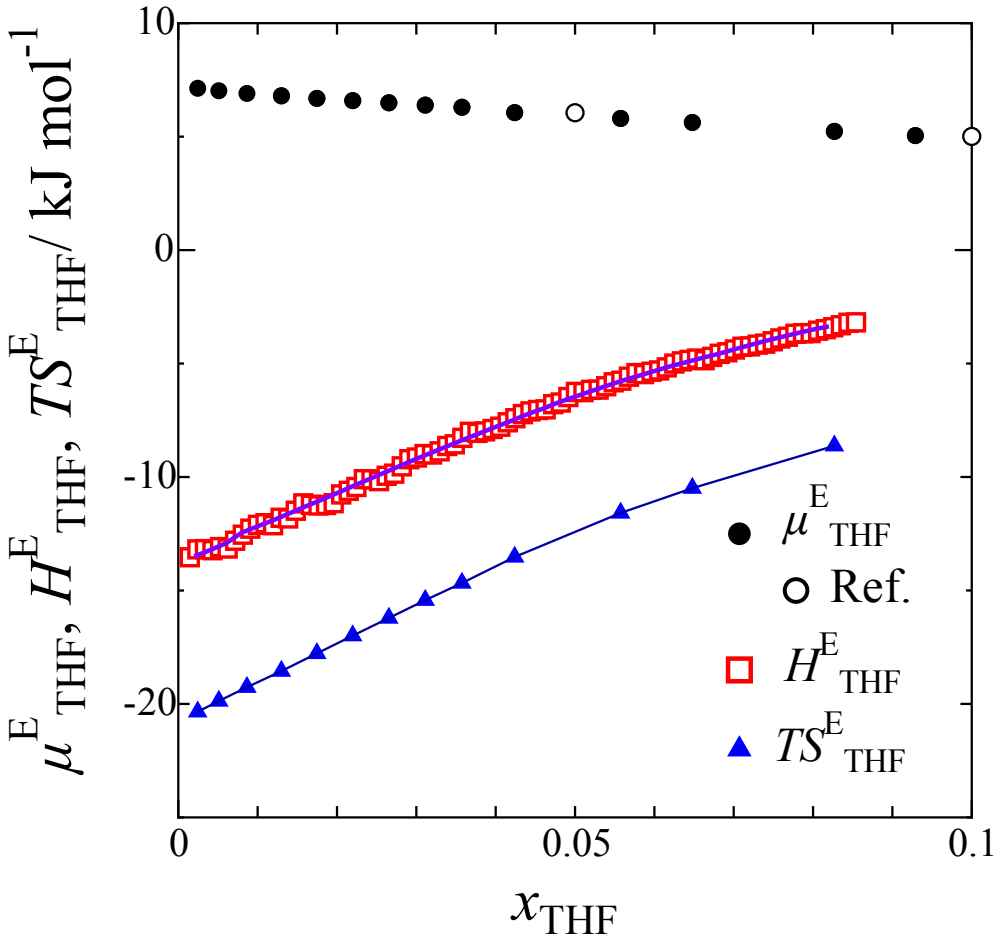

Fig. III-3. The mole-fraction dependence of H^E_{THF} (triangle), S^E_{THF} (square), μ^E_{THF} (filled circle) and 25 °C. Open circles are reference of μ^E_{THF} in [44]

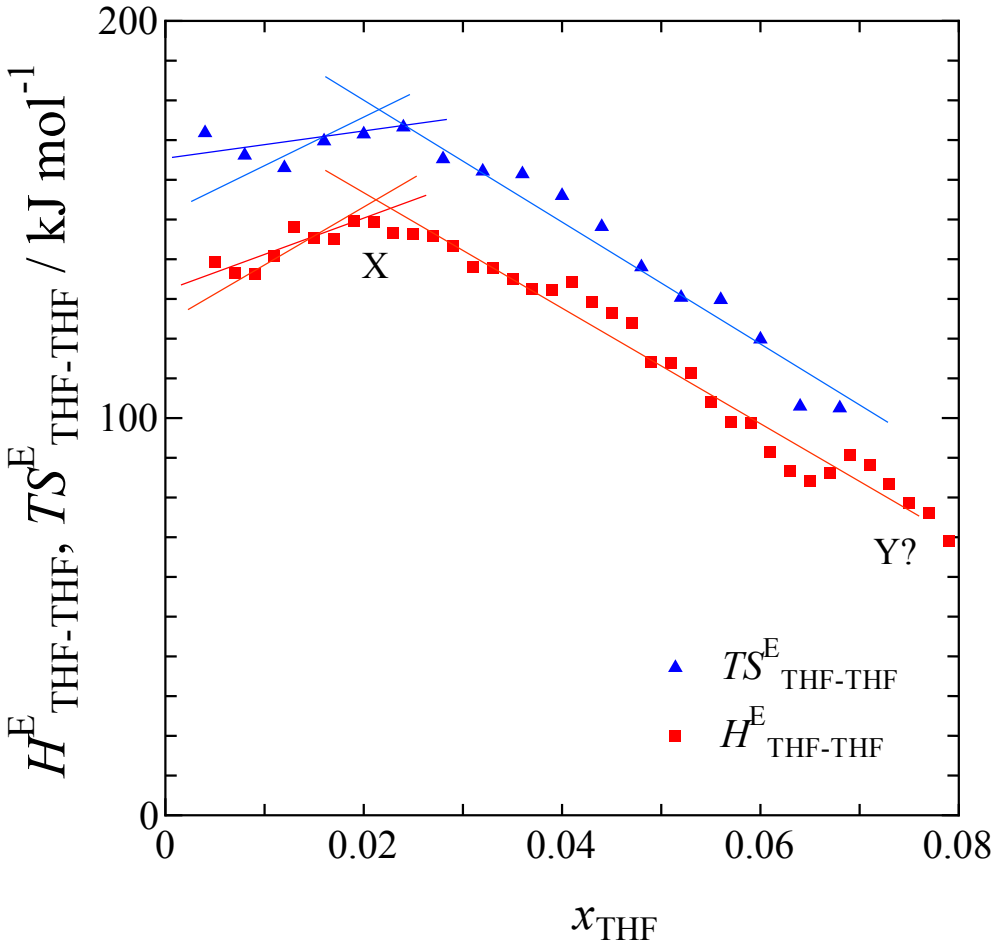

Fig. III-4. The mole-fraction dependence of $H^{E}_{THF-THF}$ and $S^{E}_{THF-THF}$ in THF aqueous solution at 25 °C. Point Y is not apperant with in the measured data.

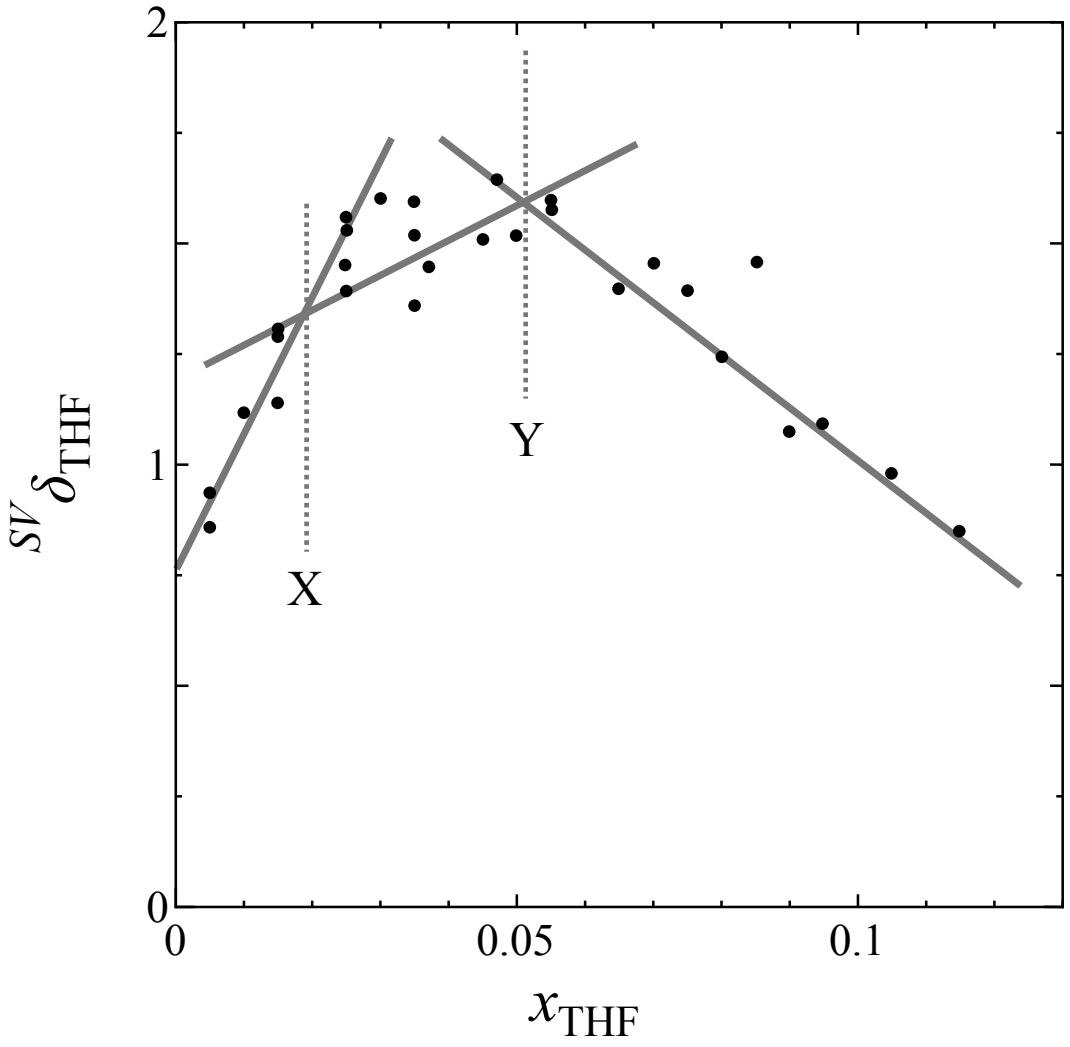

Fig. III-5. The result of $^{SV}\delta_{THF}$ measurement at 25 ˚C.

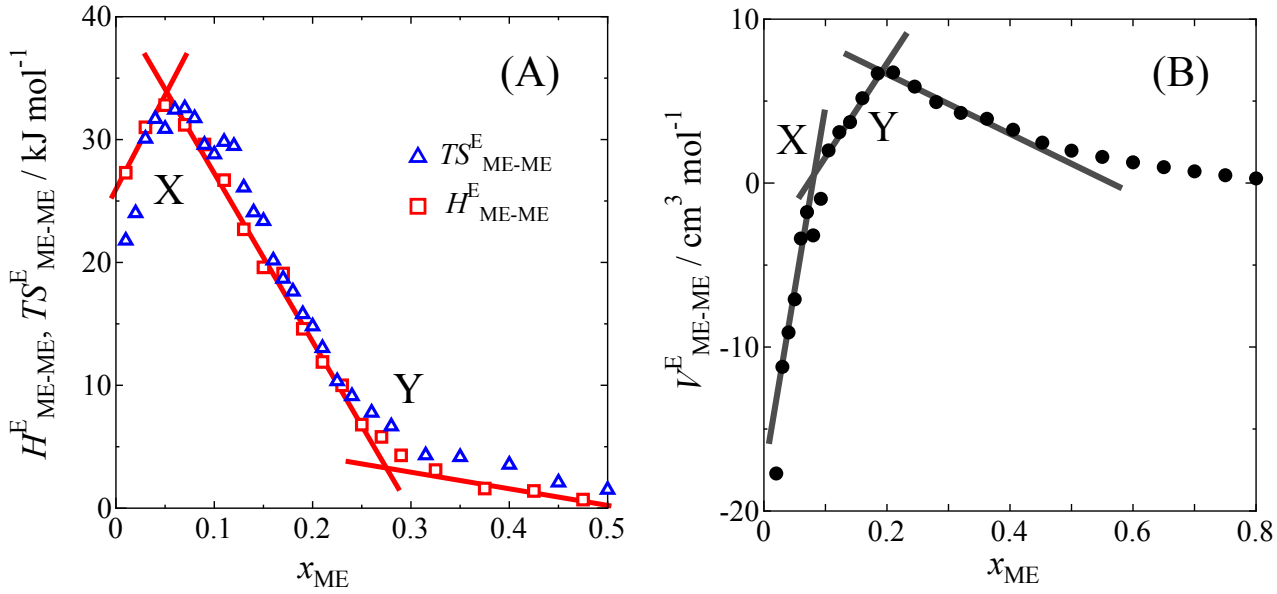

Fig. III-6. The x_{ME}-dependence of (A) H^{E}_{ME-ME}, TS^{E}_{ME-ME},[48] and (B) V^{E}_{ME-ME} [46] in Methanol (ME) aqueous solution For H^{E}_{ME-ME} and TS^{E}_{ME-ME}, there are peak-type anomaly at X and end of peak at Y. For V^{E}_{ME-ME}, there is a peak-type anomaly at Y, and bend-type anomaly at Y.

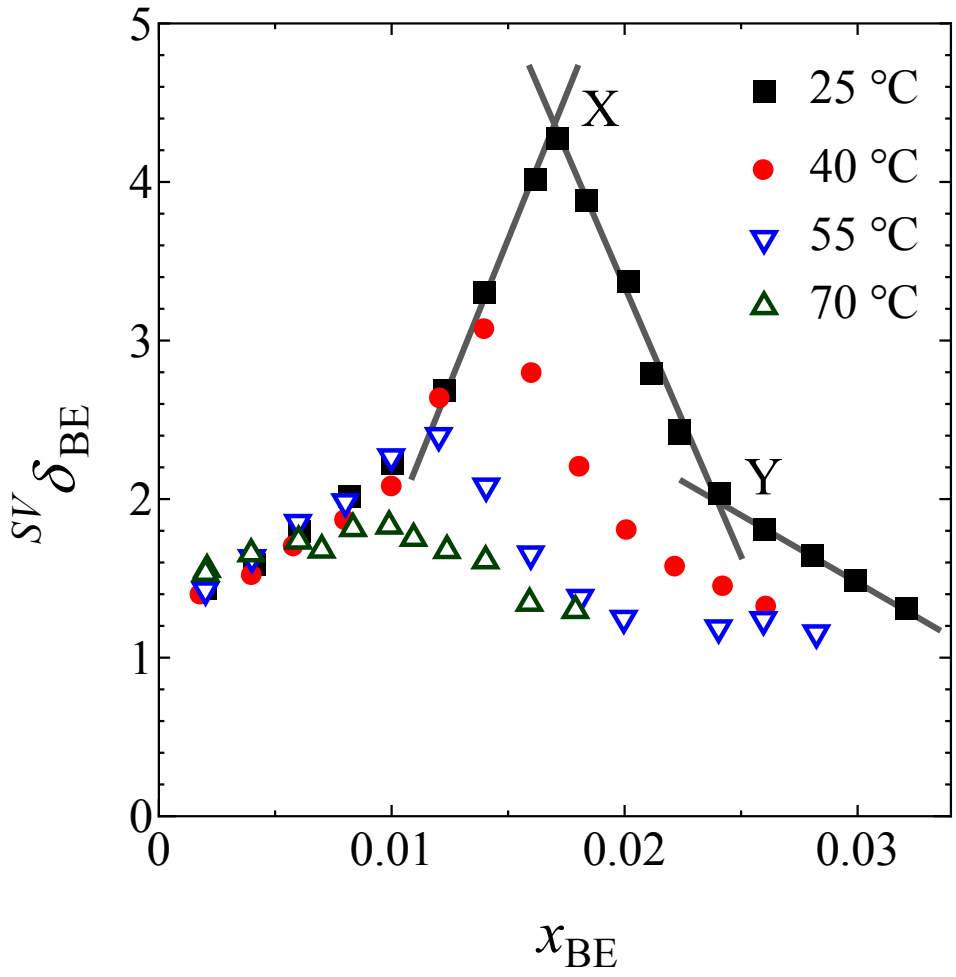

Fig. III-7. The result of $^{SV}\delta_{BE}$ measurement for 2-butoxyethanol aqueous solution at various temperatures.

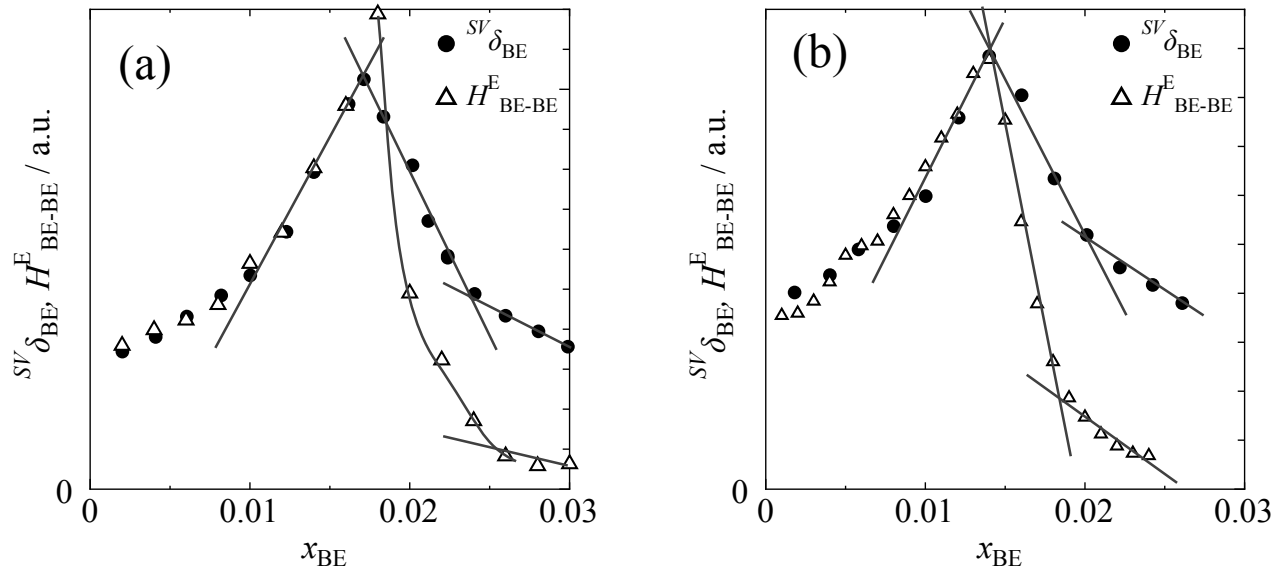

Fig. III-8. The comparison between $^{SV}\delta_{BE}$ and $H^{E}_{BE\text{-}BE}$ at 25 ˚C (a) and 40 ˚C (b).

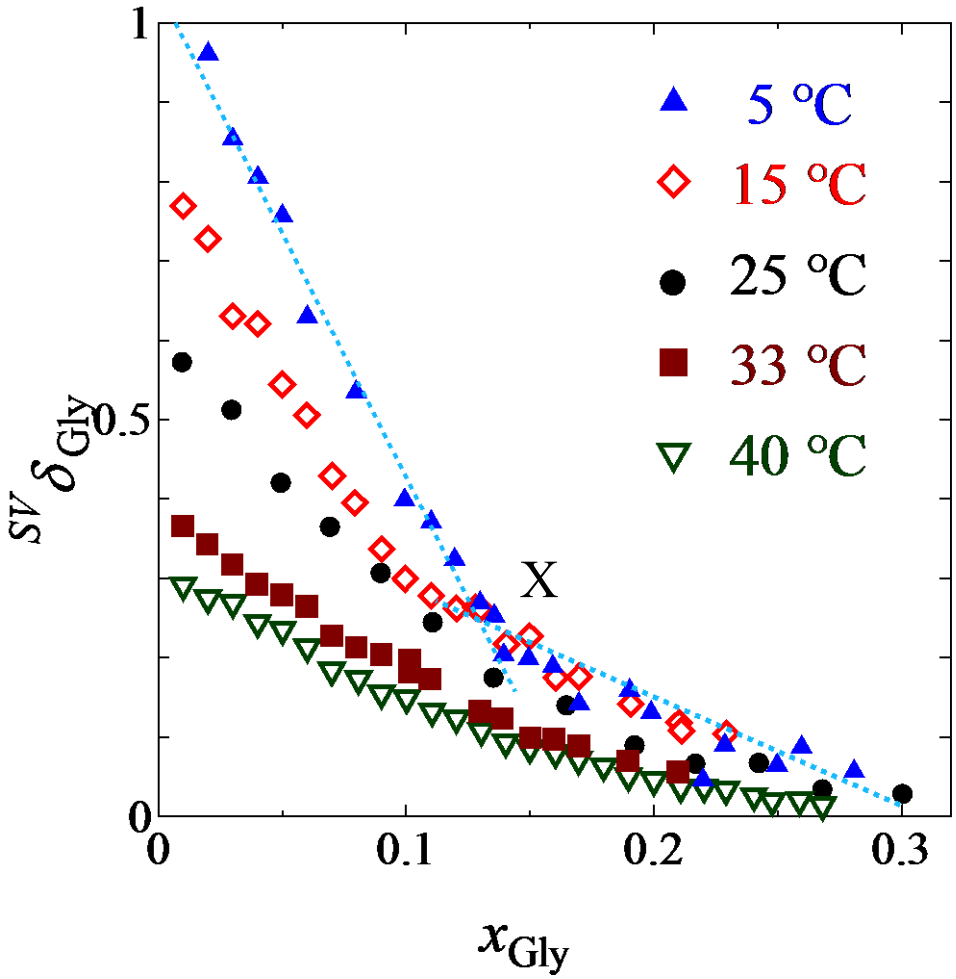

Fig. III-9. The result of $^{SV}\delta_{Gly}$ measurement for glycerol aqueous solution at various temperatures.

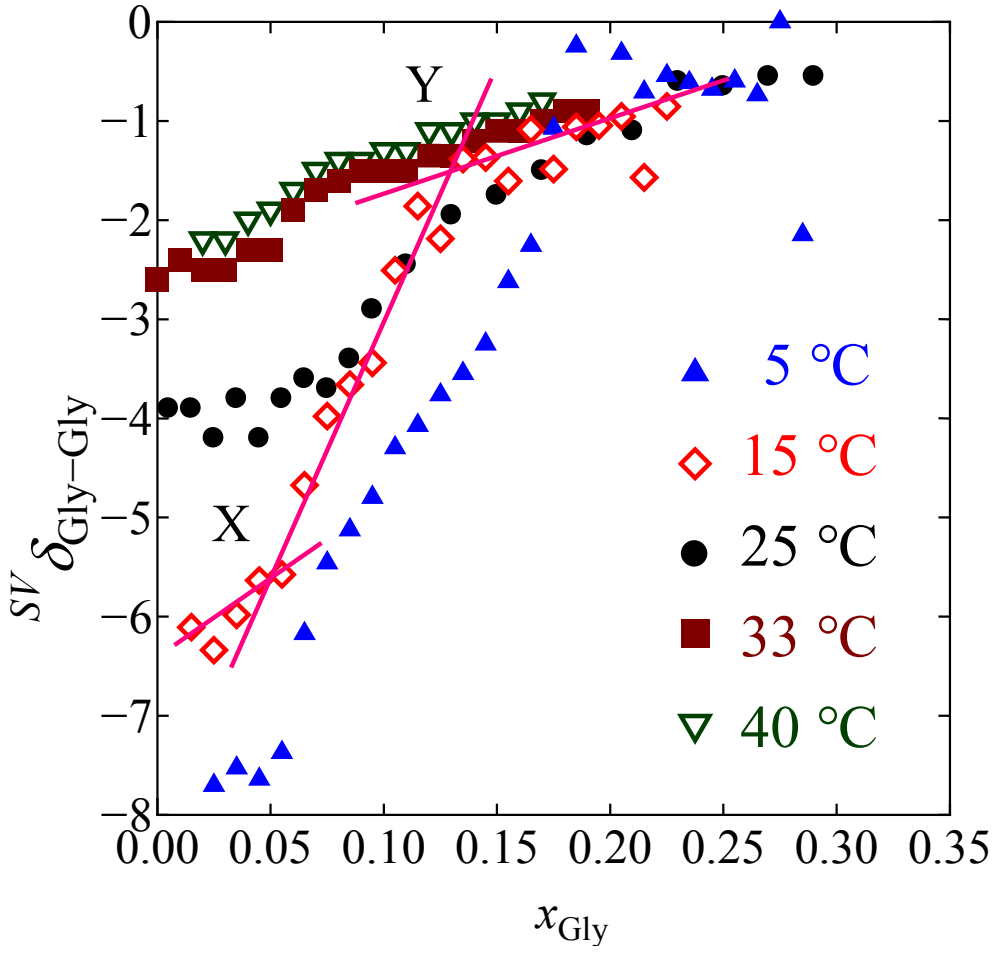

Fig. III-10. The mole-fraction dependence of $^{SV}\delta_{\mathrm{Gly\text{-}Gly}}$.

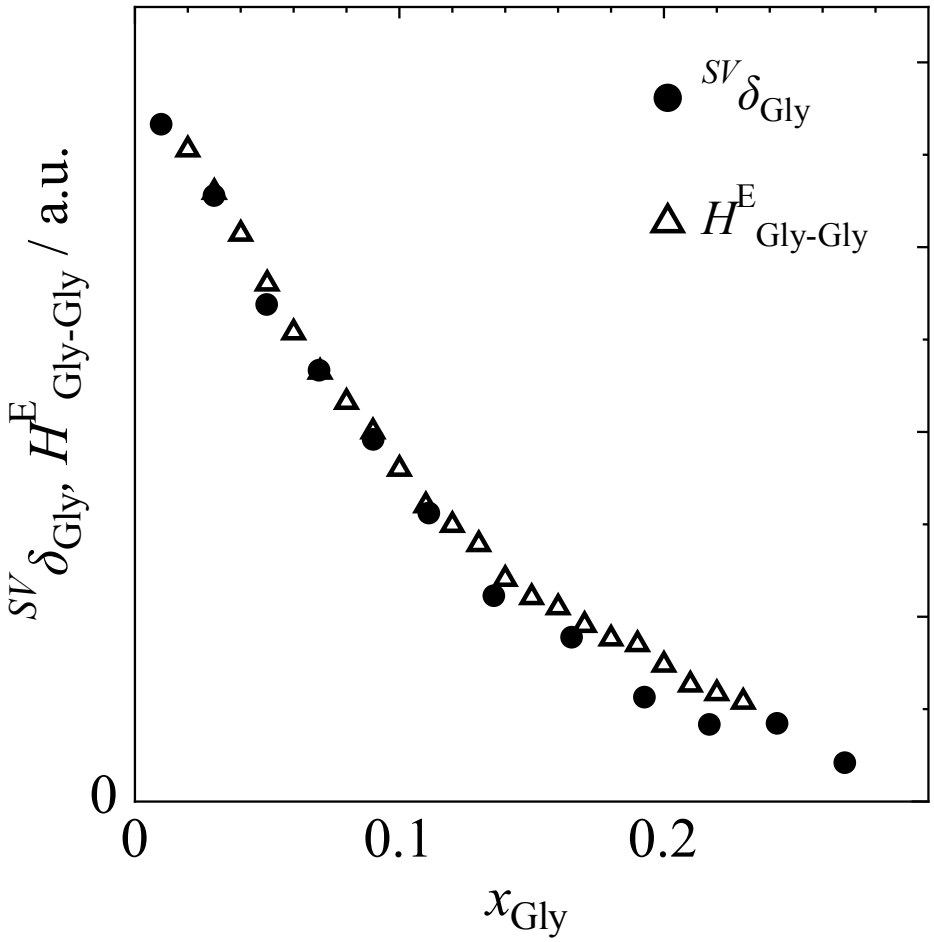

Fig. III-11. The comparison between $^{SV}\delta_{Gly}$ and $H^{E}_{Gly\text{-}Gly}$ at 25 ˚C.

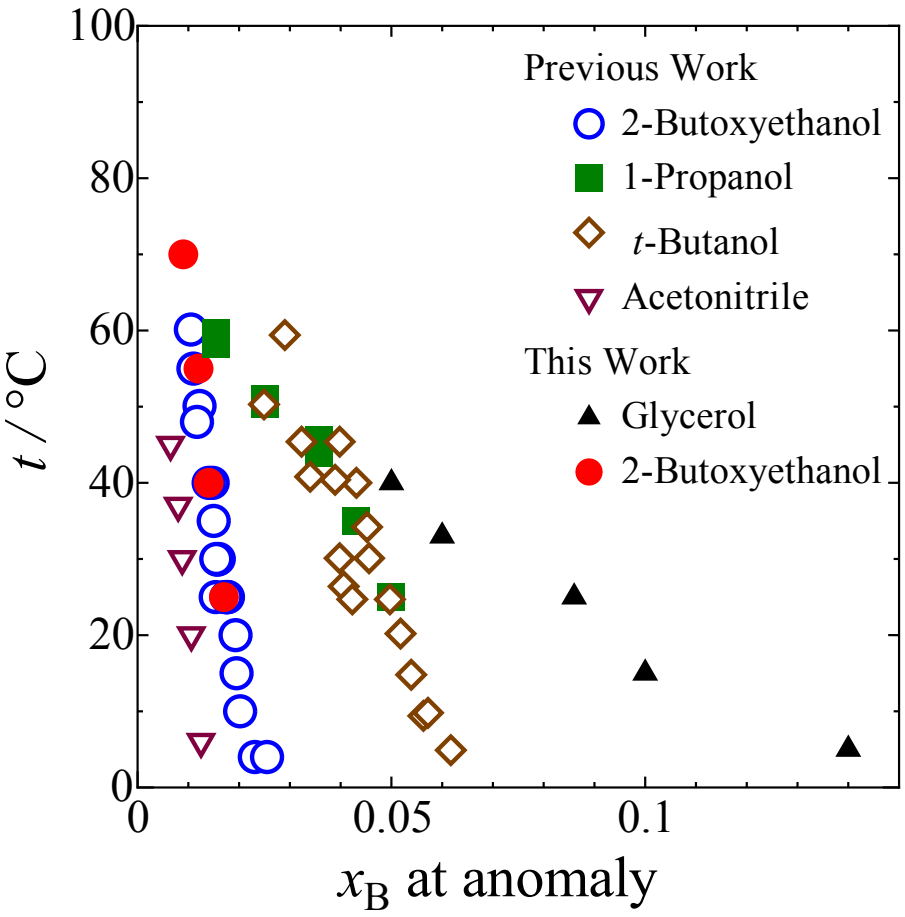

Fig. III-12. The relationship between x_B at anomaly and temperature.

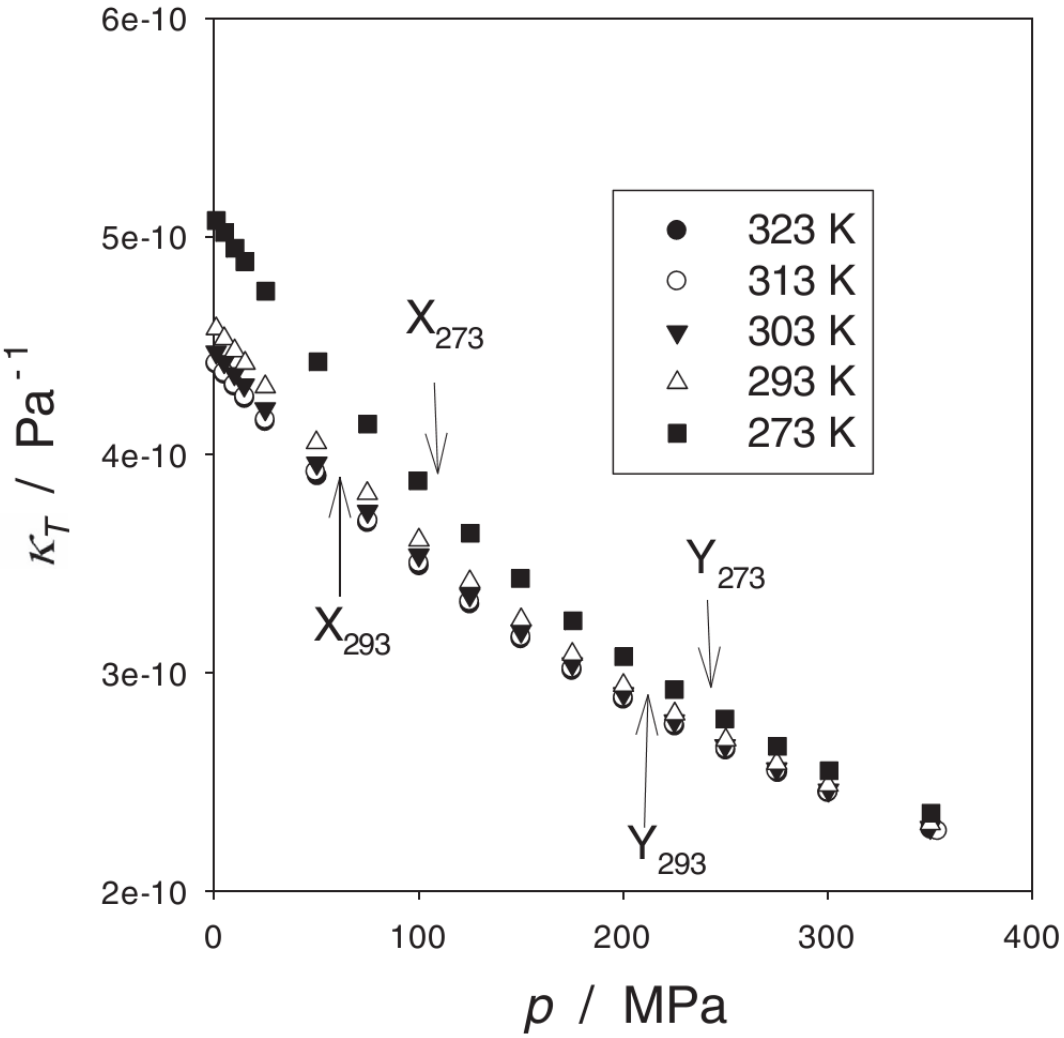

Fig. III-13. The calculated κ_T vs.p for pure water.

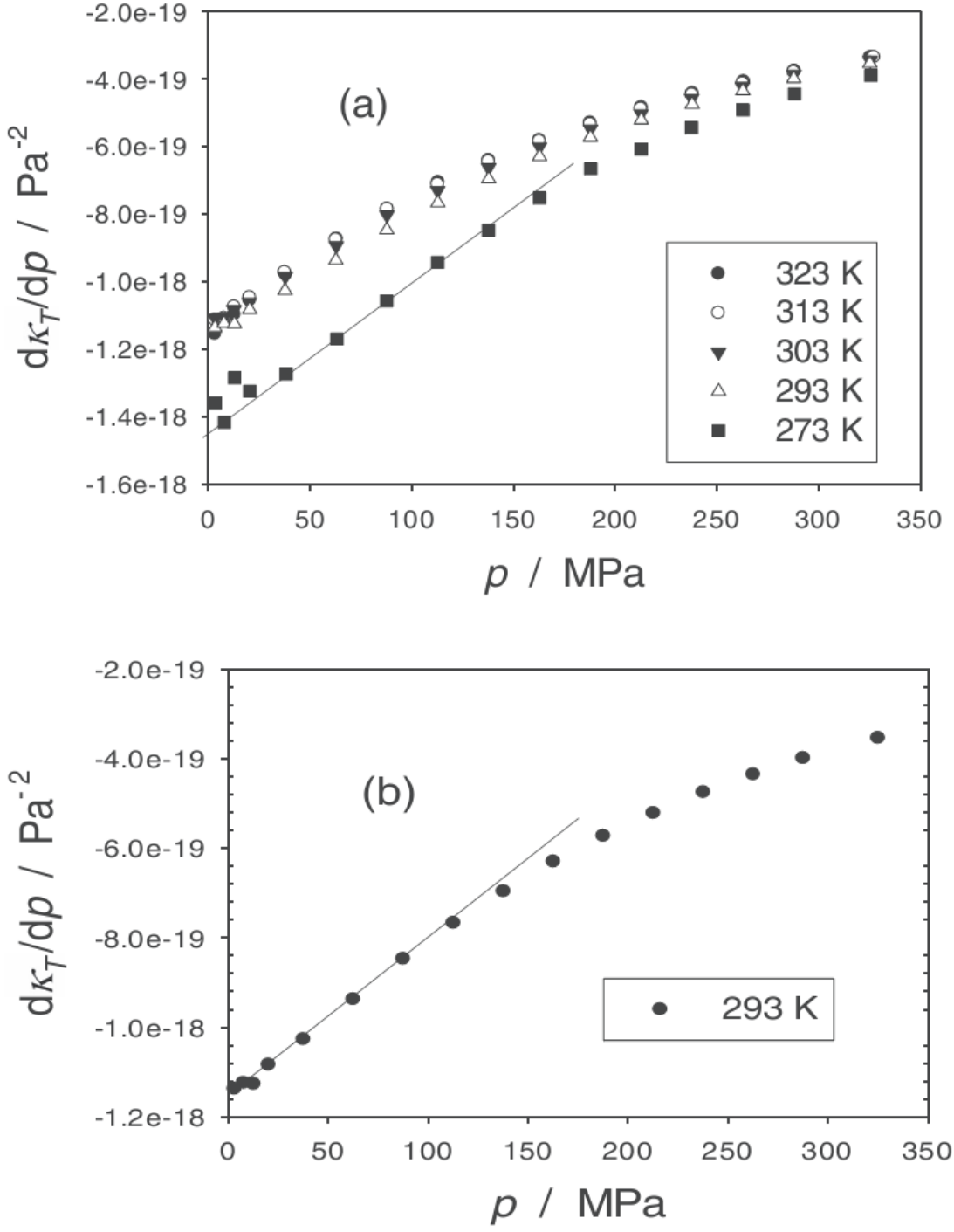

Fig. III-14. The $d\kappa_T / dp$ vs.p for pure water.

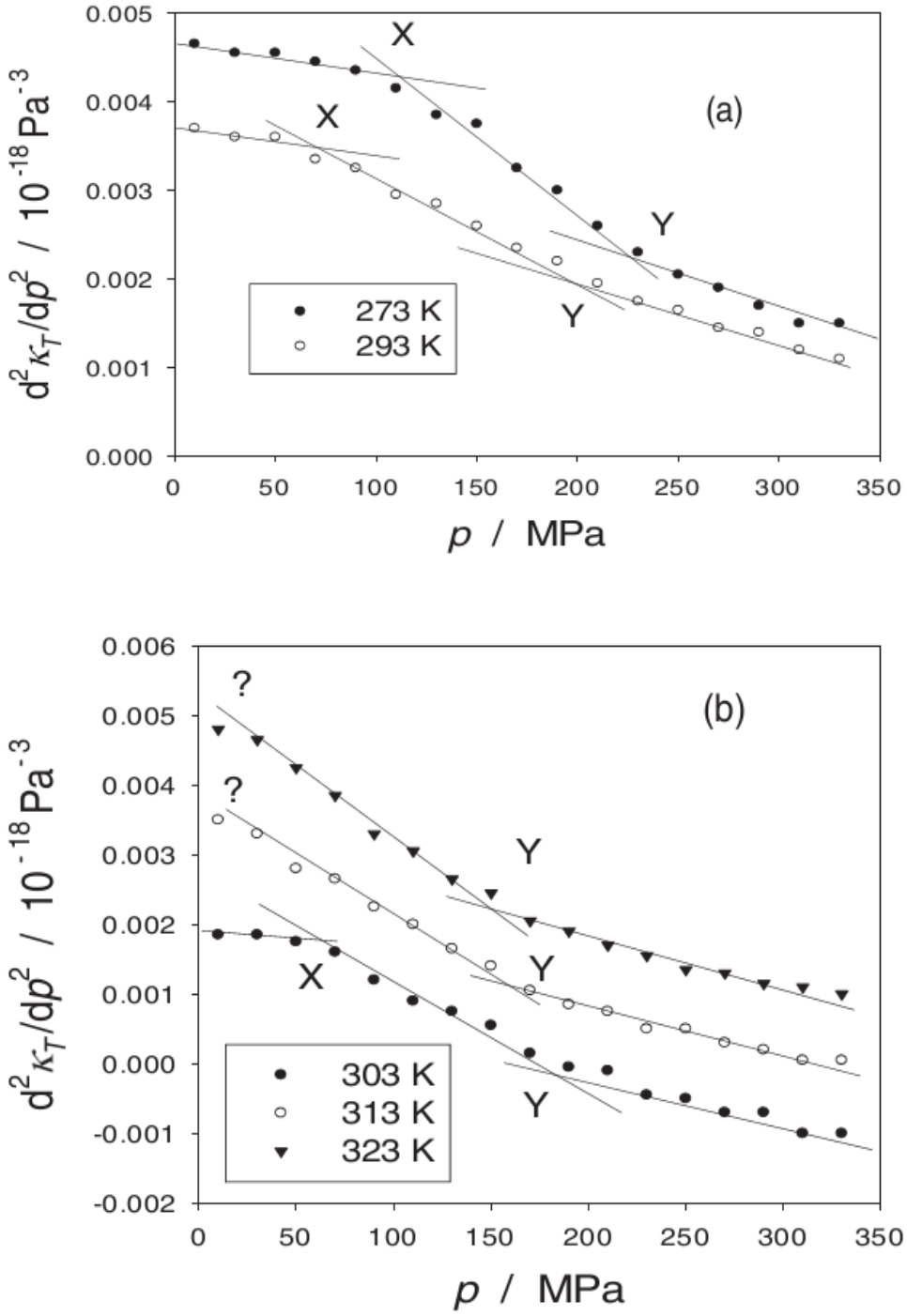

Fig. III-15. The $d^2\kappa_T$ / dp^2 vs.p for pure water.

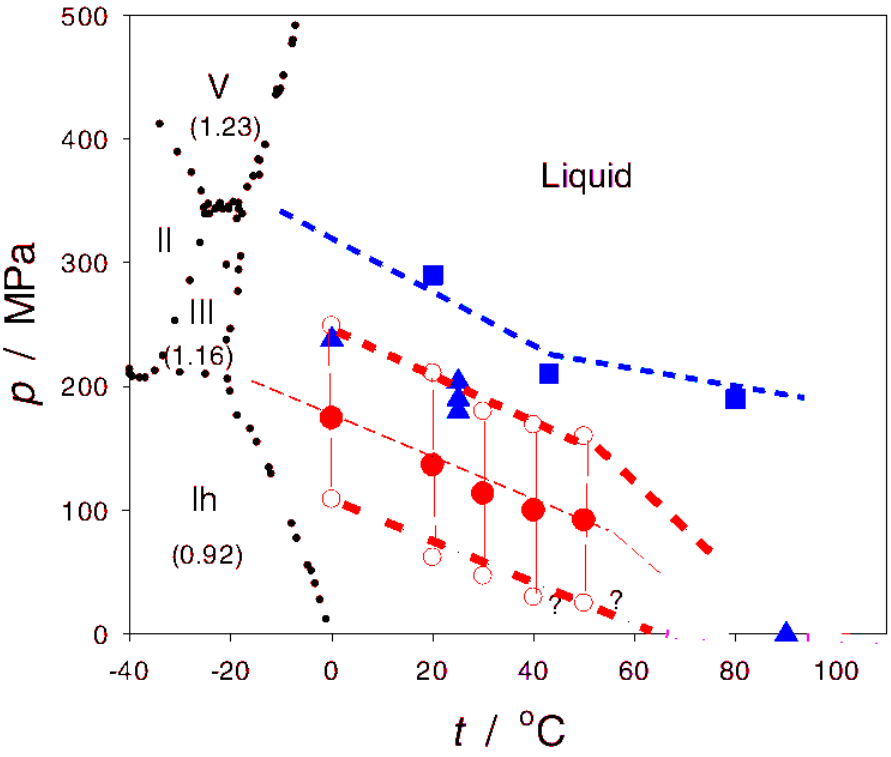

Fig. III-16. Phase diagram of water, and regions of liquid water with different molecular organization. Filled black circles; solid-liquid and solid-solid phase boundaries. [60][61] Blue broken line; boundary between “high-” and “low-density” liquid. [62] Blue filled square; from Brillouin scattering. [63] Blue filled triangle; from femtosecond pump-probe spectroscopy. [62] Red hollow circles, red filled circles, red lines and purple lines; this work. For the thick dot-dash line for point X, thick broken line for point Y, and thin broken line for mid-points of X and Y, see text for details

IV. Conclusion

For studies of the mixing scheme in aqueous solutions, the higher order derivatives of Gibbs energy were obtained, because they contain more detailed information about the system than lower order derivatives. As a result, the third derivatives of Gibbs energy for various aqueous solutions were found to show anomalies which apparently mark the crossover of the mixing schemes in aqueous solutions.

(a) Third Derivatives of G^E in Tetrahydrofuran Aqueous Solution

The various third derivatives were obtained for aqueous solution of tetrahydrofuran (THF) which has a cyclic ether. Two such third derivatives, $H^E_{THF\text{-}THF}$ and $TS^E_{THF\text{-}THF}$, were obtained from isothermal titration calorimetry and vapor pressure measurements. In the mole-fraction dependences of $H^E_{THF\text{-}THF}$ and $TS^E_{THF\text{-}THF}$, the peak-type anomalies are apparent just as for a hydrophobic solute, and the tops of weak peaks are at $x_{THF} = 0.02$, which is called as point X. $V^E_{THF\text{-}THF}$ was calculated from V^E data by Kiyohara et al.[45] The mole fraction dependence of $V^E_{THF\text{-}THF}$ shows a bend-type anomaly at 0.020 followed by a weak peak at $x_{THF} = 0.044$ presumably corresponding to the point X and Y of $H^E_{THF\text{-}THF}$. ${}^{SV}\delta_{THF}$ was measured directly. The mole-fraction dependence of ${}^{SV}\delta_{THF}$ displays the bend-type anomaly at $x_{THF} = 0.02$, followed by the peak-type anomaly at $x_{THF} = 0.052$. It was thus concluded that point X, the beginning of

crossover of Mixing Scheme, is at 0.02 and point Y, the end of the process, at 0.04 - 0.05. Namely, the patterns of $H^{E}_{THF\text{-}THF}$ and $TS^{E}_{THF\text{-}THF}$ are not the same as those of $V^{E}_{THF\text{-}THF}$ and ${}^{SV}\delta_{THF}$. For aqueous methanol (ME), $H^{E}_{ME\text{-}ME}$ and $TS^{E}_{ME\text{-}ME}$ showed the peak-type anomalies, while that of $V^{E}_{ME\text{-}ME}$ displayed the bend-type anomaly first followed by the peak. This similarity suggests THF is not a hydrophobe nor hydrophile but is an amphiphile. The same should be true for methanol.

(b) Temperature Dependence of Third Derivatives in Some Aqueous Solutions

The ${}^{SV}\delta_{B}$ is directly measured by the laboratory-made equipment for 2-butoxyethanol (BE) and Glycerol (Gly) aqueous solutions at several temperatures. ${}^{SV}\delta_{BE}$ for 2-butoxyethanol has a peak-type anomaly. This anomaly indicates that 2-butoxyethanol is hydrophobic in nature in aqueous solution. ${}^{SV}\delta_{Gly}$ for glycerol show a bend-type anomaly which indicates that glycerol is hydrophilic. These loci against temperature form a curve, which is called the “Koga line” for a given solute. Regardless of the nature of the solute, extrapolation of the Koga lines to $x_B = 0$ points to 60 – 70 ˚C.

In pure water system, the p derivative of κ_T, $\partial\kappa_T/\partial p$, which is a third derivative of G increases as pressure increases. The increase is almost linearly at first and starts to bend down at a specific point depending on temperature. The double p derivative of κ_T which is a fourth derivative displays a step-type anomalies beginning at point X and ending at Y. This suggests that the third

derivative quantities, $\partial\kappa_T / \partial p$, shows the bend-type anomaly just as the case of ${}^{SV}\delta_{\mathrm{Gly}}$ for glycerol-water. Extrapolation of the locus of point X in the *p*-*T* plane to the atmospheric pressure (0.1 MPa) points to 60 – 70 ˚C that is the same value obtained at the infinite dilution value of the Koga lines. This suggests that the molecular organization of the bulk H_2O below the Koga line in the x_B-*T* plane in aqueous solutions and that of pure H_2O in the *p*-*T* plane below point X for a given temperature must be the same. Namely the hydrogen bond network percolation is intact in both regions in the *p*-*T* field and the x_B-*T* field.

V. References

[1] Y. Koga, *Solution Thermodynamics and its Application to Aqueous Solutions: A Differential Approach*. (Elsevier, Amsterdam, **2007**), Chapter IV

[2] W. C. Röntgen, *Ann, Phys*, **1982**, *45*, 91-97

[3] J. D. Bernal and R. H. Fowler, *J. Chem. Phys.*, **1933**, *1*, 515-548

[4] M. P. Bassez , J. Lee , G. W. Robinson, *J. Phys. Chem.*, **1987**, *91*, 5818–5825

[5] M. Vedamuthu , S. Singh , G. W. Robinson, *J. Phys. Chem*., **1994,** *98*, 8591–8593

[6] M. Vedamuthu , S. Singh , G. W. Robinson, *J. Phys. Chem*., **1995**, *99*, 9263–9267

[7] M. G. Sceats1 and S. A. Rice, *J. Chem. Phys.*, **1980**, *72*, 6183

[8] H. E. Stanley and J. Teixeira, *J. Chem. Phy.*, **1980**, *73*, 3404-3422

[9] N. G. Parsonage and L. A. K. Stavely, *Disorder in Crystals,* Clarendon, Oxford, **1978**, *84*.

[10] L. D. Landau and E. M. Lifshitz, *Statistical Physics*, Addison-Wesley, **1969**.

[11] W. Siu, Y. Koga. *Can*. *J. Chem.* **1989**, *67*, 671–676.

[12] P. Westh, E. L. Rasmussen, Y. Koga, J. *Solution Chem*. **2011**, *40*, 93-105

[13] E. C. H. To, J. V. Davies, M. Ticker, P. Westh, C. Trandum, K. S. H. Suh, and Y. Koga, *Journal of Solution Chemistry*, **1999**, , 1137-1157

[14] R. H. Stokes, K. N. Marsh, R. P. Tomlins, *J. Chem. Thermodyn.* **1969**, *1*, 211–221.

[15] J. V. Davies, F. W. Lau, L. T. N. Le, Y. Koga, *Can*. *J. Chem*. **1992**, *70*, 2659-2663.

[16] Y. Koga, *Can*. *J*. *Chem*. **1999**, *77*, 2039-2045.

[17] Masami Takenaka, Reiji Tanaka and Sachio Murakami, *J. Chem. Thermodynamics* **1980**, *12*, 849-855.

[18] Y. Koga, *Solution Thermodynamics and its Application to Aqueous Solutions: A Differential Approach*. Chapter V.

[19] H. S. Frank, M. W. Evans, *J*. *Phys*. *Chem*. **1945**, *13*, 507-532

[20] Y. Koga. *J. Cryst. Soc. Jpn.* **1995**, *37*, 172-182

[21] Y. Koga, Nishikawa, K., Westh, P. *J. Phys. Chem. A* **2004**, *108*, 3873–3877.

[22] Y. Koga, *Solution Thermodynamics and its Application to Aqueous Solutions: A Differential Approach*. Chapter VI.

[23] Y. Koga, *Solution Thermodynamics and its Application to Aqueous Solutions: A Differential Approach*. Chapter VII.

[24] T. Makino, T. Sugahara, K. Ohgaki, *J. Chem. Eng. Data*, **2005**, *50*, 2058-2060.

[25] Y. Koga, William W. Y. Siu, T. Y. H. Wong, *J*. *Phys*. *Chem*. **1990**, *94*, 3879-3881

[26]Y. Koga. *The Journal of Physical Chemistry*, **1992**, *96*, 10466-10468

[27] Y. Koga, P. Weth, Y. Moriya, K. Kawasaki, T. Atake, *J*. *Phys*. *Chem*. **2009**, *113*, 5885-5890

[28] K. Yoshida, S. Baluja, A. Inaba, K. Tozaki, Y. Koga, *J. Solution Chem.* **2011**, *40*, 1271–1278.

[29] F. Franks, Water: A comprehensive treatise, Plenum, New York, **1972**, Vol.1-7,

[30] T. Sato, R. Buchner, *J. Mol. Liq.*, **2005**, *117*. 23-29

[31] S. Dixit, W. C. K. Poon and J. Crain, *J. Phys.: Condens. Matter*. **2000**, *12*, L323–L328

[33] J. L. Finney, A. K. Soper, *Chem. Soc. Rev*., **1994**, *23*, 1-10

[32] H. S. Frank, M. W. Evans, *J. Chem. Phys*. **1945**, *13*, 507-532

[34] H. J. Bakker, *J. Chem. Rev.* **2008**, *108*, 1456-1473

[35] A. A. Bakulin, C. Liang, T C.Jansen, D. A. Wiersma, H. J. Bakker, M. S. Pshenichnikov, *Acc. Chem. Res.*, **2009**, *42*, 1229-1238

[36] C. Petersen, A. A. Bakulin, V. G. Pavelyev, M. S. Pshenichnikov, H. J. Bakker, *J. Chem. Phys.*, **2010**, *133*, 164514

[37] K. Mazur, I. A. Heisler, and S. R. Meech, *J. Phys. Chem. B*, **2011**, *115*, 2563–2573

[38] N. Galamba, *J. Phys. Chem. B*, **2013**, *117*, 2153-2159

[39] M. P. S. Mateus, N. Galamba, B. J. Costa Cabral, J. Chem. Phys. **2012**, *136*, 014507.

[40] T. M. Raschke, M. Levitt, *PNAS*, **2005**, *102*, 6777-6782

[41] Y. Koga, in *Comprehensive Handbook of Calorimetry&Thermal Analysis*, edited by M. Sorai (Wiley, Chichester, **2004**), pp. 195–199.

[42] Ch. G. Boissonnas, *Helv. Chim. Acta*, **1939**, *22*, 541-547.

[43] Y. Koga. *J. Phys. Chem***. 1991**, *95*, 4119–4126.

[44] R. Signer, H. Arm and H. Daeniker, *Helv. Chim. Acta*, **1969**, *52*, 2347–2351.

[45] O. Kiyohara, P. J. D'arcy, G. C. Bencon, *Can. J. Cchem*. **1978**, *56*, 2803-2807

[46] G. C. Benson, O. Kiyohara, *Journal of Solution Chem.*, **1980**, *9*, 791-804

[47] E. C. H. To, J. V. Davies, M. Ticker, P. Westh, C. Trandum, K. S. H. Suh, Y. Koga *Journal of Solution Chemistry*,**1999**. *28*, 10

[48] A. W. C. Ho, F. W. Lau, P. Westh, Y. Koga, *Canadian Journal of Chemistry*, **1996**, *74*, 713-721

[50] K. Yoshida, S. Baluja, A. Inaba, Y. Koga. *J. Chem. Phys.* **2011**, *134*, 214502–214502.

[51]Y. Koga. *The Journal of Physical Chemistry*, **1992**, *96*, 10466-10468

[52] Y. Koga., Westh, P., Yoshida, K., Inaba, A., Nakazawa, Y. *AIP Adv.* **2014**, *4*, 097116.

[53] Ter Minassian, L. *J. Chem. Phys.* **1981**, *75*, 3064.

[54] G.S. Kell, *J. Chem. Eng. Data*, **1975**, *20*, 97-105

[55] G.S. Kell, *J. Chem. Eng. Data*, **1967**, *12*, 66-69

[56] B. Guignon, C. Aparicio, and P. D. Sanz, *J. Chem. Eng. Data*, **2010**, *55*, 3338

[57] C.-W. Lin and J. P. M. Trusler, *J. Chem. Phys.* **2012**, *136*, 094511

[58] L. D. Landau and E. M. Lifshitz, *Statistical Physics*, Addison-Wesley, **1969**.

[59] M. T. Parsons, P. Westh, P. J. V. Davies, C. Trandum, E. C. H. To, W. M. Chiang, E. G. M. Yee, Y. Koga, *J. Solution Chem*, **2001**, *30*, 1007-1028.

[60] Water, in the Liquid and Five Solid Forms, under Pressure. W. Bridgeman, Proc. *Am. Acad. Arts Sci.* **1912**, *47*, 441.

[61] G. S. Kell and E. Whalley, *J. Chem. Phys*. **1968**, *48*, 2359.

[62] A. M. Saitta and F. Datchi, *Phys. Rev*. **2003**, *67*, 020201(R)

[63] F. Li, Q. Cui, Z. He, J. Zhang, Q. Zhou, G. Zou, and S. Sasaki, *J. Chem. Phys*.**2005**, *123*, 174511.

[64] S. Fanetti, A. Lapini, M. Pagliai, M. Citroni, M. Di Donato, S. Scandolo, R. Righini, and R. Bini, *J. Phys. Chenistry Lett*., **2014**, *5*, 3804-3809

VI. Appendix – Experimental Data

(a) H^{E}_{B}

● Tetrahydrofuran

Table 1. The mole-fraction dependence of H^{E}_{THF} in THF aqueous solution at 25 °C.

x_{THF}	H^{E}_{THF} /kJ mol^{-1}	x_{THF}	H^{E}_{THF} /kJ mol^{-1}	x_{THF}	H^{E}_{THF} /kJ mol^{-1}
0.00145	13.53	0.03007	9.141	0.05870	5.464
0.00240	13.19	0.03103	8.989	0.05965	5.359
0.00336	13.18	0.03198	9.006	0.06061	5.302
0.00431	13.22	0.03294	8.868	0.06156	5.168
0.00526	13.09	0.03389	8.632	0.06252	4.999
0.00622	13.15	0.03484	8.556	0.06347	4.902
0.00717	12.81	0.03580	8.271	0.06442	4.837
0.00813	12.54	0.03675	8.008	0.06538	4.779
0.00908	12.28	0.03771	8.054	0.06633	4.853
0.01004	12.10	0.03866	7.987	0.06729	4.704
0.01099	12.04	0.03961	7.882	0.06824	4.567
0.01194	12.12	0.04057	7.782	0.06919	4.503
0.01290	11.79	0.04152	7.588	0.07015	4.379
0.01385	11.83	0.04248	7.407	0.07110	4.257
0.01481	11.49	0.04343	7.226	0.07206	4.243
0.01576	11.16	0.04439	7.106	0.07301	4.168
0.01671	11.22	0.04534	7.046	0.07397	4.122
0.01767	11.25	0.04629	7.019	0.07492	4.019
0.01862	11.23	0.04725	6.788	0.07587	3.892
0.01958	11.15	0.04820	6.718	0.07683	3.817
0.02053	10.76	0.04916	6.475	0.07778	3.687
0.02149	10.61	0.05011	6.249	0.07874	3.665
0.02244	10.44	0.05107	6.259	0.07969	3.657
0.02339	10.10	0.05202	6.157	0.08064	3.551
0.02435	10.10	0.05297	6.148	0.08160	3.482
0.02530	10.18	0.05393	6.000	0.08255	3.400

0.02626	9.944	0.05488	5.824	0.08351	3.310
0.02721	9.853	0.05584	5.754	0.08446	3.201
0.02816	9.527	0.05679	5.577	0.08542	3.183
0.02912	9.214	0.05774	5.418		

(b)TS^{E}_{B}

- Tetrahydrofuran

Table 2. The mole-fraction dependence of TS^{E}_{THF} in THF aqueous solution at 25 °C.

$x_{THF-THF}$	$TS^{E}_{THF-THF}$ /kJ mol^{-1}	$x_{THF-THF}$	$TS^{E}_{THF-THF}$ /kJ mol^{-1}	$x_{THF-THF}$	$TS^{E}_{THF-THF}$ /kJ mol^{-1}
0.00244	-20.35	0.02198	-16.99	0.05575	-11.58
0.00510	-19.87	0.02654	-16.21	0.06478	-10.49
0.00865	-19.26	0.03112	-15.43	0.08269	-8.62
0.01299	-18.55	0.03575	-14.67		
0.01747	-17.77	0.04240	-13.52		

(c) $H^{E}_{B\text{-}B}$

● Tetrahydrofuran

Table 3. The mole-fraction dependence of $H^{E}_{THF\text{-}THF}$ in THF aqueous solution at 25 ˚C.

x_{THF}	$H_{THF\text{-}THF}$ / kJ mol^{-1}	x_{THF}	$H_{THF\text{-}THF}$ / kJ mol^{-1}	x_{THF}	$H_{THF\text{-}THF}$ / kJ mol^{-1}
0.005	139.30	0.031	138.08	0.057	99.02
0.007	136.54	0.033	137.80	0.059	98.81
0.009	136.26	0.035	135.10	0.061	91.55
0.011	140.93	0.037	132.41	0.063	86.67
0.013	148.05	0.039	132.14	0.065	84.15
0.015	145.29	0.041	134.26	0.067	86.30
0.017	144.99	0.043	129.20	0.069	90.77
0.019	149.60	0.045	126.54	0.071	88.26
0.021	149.30	0.047	123.89	0.073	83.43
0.023	146.55	0.049	114.12	0.075	78.63
0.025	146.25	0.051	113.88	0.077	76.15
0.027	145.95	0.053	111.27	0.079	69.08
0.029	143.22	0.055	103.95		

● Methanol

Table 4. The mole-fraction dependence of $H^{E}_{ME\text{-}ME}$ in methanol aqueous solution at 25 ˚C.

x_{ME}	$H_{ME\text{-}ME}$ / kJ mol^{-1}	x_{ME}	$H_{ME\text{-}ME}$ / kJ mol^{-1}	x_{ME}	$H_{ME\text{-}ME}$ / kJ mol^{-1}
0.01	27.3	0.17	19.1	0.375	1.6
0.03	31	0.19	14.6	0.425	1.4
0.05	32.8	0.21	11.9	0.475	0.70
0.07	31.2	0.23	10	0.525	0.60
0.09	29.6	0.25	6.8	0.575	0.34
0.11	26.7	0.27	5.8	0.625	0.45
0.13	22.7	0.29	4.3	0.675	0.35

0.15	19.6	0.325	3.1	0.725	0.28

(d) $TS^{E}_{B\text{-}B}$

● Tetrahydrofuran

Table 6. The mole-fraction dependence of $TS^{E}_{THF\text{-}THF}$ in THF aqueous solution at 25 °C.

x_{ME}	$TS_{THF\text{-}THF}$ / kJ mol^{-1}	x_{ME}	$TS_{THF\text{-}THF}$ / kJ mol^{-1}	x_{ME}	$TS_{THF\text{-}THF}$ / kJ mol^{-1}
0.004	171.81	0.028	165.24	0.052	130.35
0.008	166.16	0.032	162.14	0.056	129.8
0.012	163.02	0.036	161.47	0.06	119.85
0.016	169.74	0.04	156	0.064	102.96
0.02	171.5	0.044	148.18	0.068	102.52
0.024	173.24	0.048	138.04		

● Methanol

Table 7. The mole-fraction dependence of $TS^{E}_{ME\text{-}ME}$ in methanol aqueous solution at 25 °C.

x_{ME}	$TS_{ME\text{-}ME}$ / kJ mol^{-1}	x_{ME}	$TS_{ME\text{-}ME}$ / kJ mol^{-1}	x_{ME}	$TS_{ME\text{-}ME}$ / kJ mol^{-1}
0.01	21.78	0.13	26.10	0.28	6.67
0.02	24.01	0.14	24.08	0.32	4.30
0.03	30.07	0.15	23.38	0.35	4.16
0.04	31.68	0.16	20.16	0.4	3.54
0.05	30.88	0.17	18.68	0.45	2.09
0.06	32.43	0.18	17.63	0.5	1.50
0.07	32.55	0.19	15.80	0.55	1.04
0.08	31.74	0.20	14.80	0.63	0.68
0.09	29.58	0.21	13.04	0.7	0.48
0.10	28.80	0.23	10.33	0.85	0.15
0.11	29.82	0.24	9.12		
0.12	29.48	0.26	7.77		

(e)$V^{E}_{B\text{-}B}$

●Tetrahydrofuran

Table 8. The mole-fraction dependence of $V^{E}_{THF\text{-}THF}$ in THF aqueous solution at 25 ˚C.

x_{THF}	V^{E}_{THFTHF}	x_{THF}	V^{E}_{THFTHF}	x_{THF}	V^{E}_{THFTHF}
0.002	-124.75	0.08	32.20	0.43	1.7100
0.004	-124.50	0.085	32.94	0.44	1.6800
0.006	-111.83	0.0925	31.46	0.45	1.6500
0.008	-96.72	0.1	29.70	0.46	1.6200
0.01	-81.68	0.11	25.81	0.47	1.3250
0.012	-61.75	0.12	23.76	0.48	1.0400
0.014	-51.77	0.13	21.32	0.49	1.0200
0.016	-41.82	0.14	17.63	0.505	1.1220
0.018	-27.01	0.15	16.15	0.52	1.0920
0.02	-19.60	0.16	13.86	0.54	0.9775
0.022	-14.67	0.17	12.04	0.56	0.8470
0.024	-7.32	0.18	10.66	0.58	0.8715
0.026	-4.87	0.19	9.31	0.6	0.6800
0.028	0.00	0.2	10.00	0.62	0.4750
0.03	4.85	0.21	8.69	0.64	0.5130
0.032	9.68	0.22	7.02	0.66	0.4760
0.034	16.91	0.23	7.32	0.68	0.3840
0.036	24.10	0.24	5.70	0.7	0.2775
0.038	31.26	0.25	4.50	0.72	0.2660
0.04	36.00	0.26	4.07	0.74	0.2061
0.042	38.32	0.27	4.02	0.76	0.1440
0.044	38.24	0.28	3.96	0.78	0.1117
0.046	38.16	0.29	3.20	0.8	0.0500
0.048	38.08	0.3	3.50	0.82	0.0135
0.05	40.38	0.31	3.45	0.84	0.0320
0.052	40.29	0.32	3.06	0.86	0.0105
0.054	40.20	0.33	3.02	0.88	-0.0270
0.056	42.48	0.34	3.30	0.9	-0.0275
0.058	42.39	0.35	3.25	0.92	-0.0240

0.06	42.30	0.36	2.88	0.94	-0.0165
0.062	39.86	0.37	2.84	0.96	-0.0090
0.064	39.78	0.38	2.79	0.98	-0.0025
0.066	37.36	0.39	2.44	0.49	0.0005
0.068	34.95	0.4	1.80	0.5	0.0000
0.0715	37.14	0.41	1.77		
0.075	34.23	0.42	1.74		

(f) ${}^{SV}\delta_B$

● 2-Butoxyethanol

Table 9. The mole-fraction dependence of ${}^{SV}\delta_{BE}$ in 2-butoxyethanol aqueous solution.

25 °C		40 °C		55 °C	
x_{BE}	${}^{SV}\delta_{BE}$	x_{BE}	${}^{SV}\delta_{BE}$	x_{BE}	${}^{SV}\delta_{BE}$
0.00202	1.434	0.01400	3.068	0.00200	1.426
0.00410	1.586	0.01809	2.202	0.00597	1.851
0.00605	1.799	0.02219	1.571	0.00998	2.266
0.00820	2.019	0.02610	1.318	0.01406	2.081
0.01002	2.228	0.00181	1.394	0.01810	1.379
0.01229	2.683	0.00581	1.699	0.02596	1.238
0.01400	3.304	0.01002	2.077	0.00400	1.629
0.01618	4.014	0.00402	1.517	0.01202	2.400
0.01713	4.272	0.00802	1.864	0.01597	1.653
0.01836	3.881	0.01209	2.633	0.02823	1.155
0.02017	3.375	0.01603	2.792	0.02403	1.187
0.02116	2.795	0.02011	1.802	0.00801	1.982
0.02238	2.432	0.02425	1.447	0.01996	1.248
0.02238	2.412				
0.02406	2.035				
0.02600	1.807				
0.02806	1.645				
0.02990	1.485				
0.03210	1.311				

70 °C	
x_{BE}	${}^{SV}\delta_{BE}$
0.00207	1.556
0.00600	1.735
0.00989	1.830
0.01789	1.297
0.00201	1.533

0.00834	1.815
0.01237	1.676
0.01592	1.344
0.01403	1.611
0.01094	1.753
0.00699	1.680
0.00397	1.655

●Glycerol

Table 10. The mole-fraction dependence of ${}^{SV}\delta_{\mathrm{Gly}}$ in glycerol aqueous solution.

5 ˚C		15 ˚C		25 ˚C	
x_{G}	${}^{SV}\delta_{\mathrm{Gly}}$	x_{G}	${}^{SV}\delta_{\mathrm{Gly}}$	x_{G}	${}^{SV}\delta_{\mathrm{Gly}}$
0.0099	1.0418	0.0100	0.7692	0.0099	0.5712
0.0201	0.9611	0.0200	0.7279	0.0299	0.5110
0.0300	0.8537	0.0300	0.6305	0.0498	0.4192
0.0402	0.8050	0.0401	0.6208	0.0696	0.3637
0.0501	0.7567	0.0499	0.5440	0.0901	0.3054
0.0601	0.6295	0.0599	0.5055	0.1111	0.2433
0.0701	0.5779	0.0702	0.4289	0.1357	0.1736
0.0798	0.5346	0.0793	0.3953	0.1651	0.1386
0.0900	0.4592	0.0901	0.3368	0.1926	0.0880
0.0994	0.3985	0.0996	0.2994	0.2172	0.0650
0.1101	0.3712	0.1101	0.2778	0.2428	0.0659
0.1196	0.3238	0.1203	0.2620	0.2684	0.0328
0.1299	0.2688	0.1281	0.2631	0.3007	0.0270
0.1356	0.2525	0.1301	0.2619	0.3311	0.0135
0.1394	0.2035	0.1405	0.2170	0.3560	0.0206
0.1494	0.1987	0.1499	0.2270	0.3843	0.0087
0.1592	0.1888	0.1499	0.2270		
0.1698	0.1421	0.1605	0.1747		
0.1902	0.1587	0.1698	0.1759		
0.1912	0.0991	0.1907	0.1414		
0.1989	0.1306	0.2103	0.1181		

0.2108	0.1098	0.2112	0.1076
0.2199	0.0460	0.2292	0.1040
0.2287	0.0899		
0.2498	0.0646		
0.2597	0.0871		
0.2809	0.0566		

33 °C		40 °C	
x_G	${}^{SV}\delta_{Gly}$	x_G	${}^{SV}\delta_{Gly}$
0.0100	0.3653	0.0100	0.2909
0.0200	0.3422	0.0200	0.2745
0.0301	0.3172	0.0301	0.2686
0.0399	0.2921	0.0400	0.2440
0.0500	0.2789	0.0501	0.2354
0.0600	0.2642	0.0601	0.2131
0.0701	0.2268	0.0700	0.1837
0.0800	0.2124	0.0808	0.1727
0.0902	0.2034	0.0900	0.1546
0.1013	0.1814	0.1002	0.1488
0.1015	0.1963	0.1105	0.1323
0.1098	0.1725	0.1203	0.1236
0.1299	0.1322	0.1304	0.1077
0.1390	0.1225	0.1402	0.0935
0.1503	0.0986	0.1500	0.0857
0.1598	0.0964	0.1603	0.0797
0.1699	0.0881	0.1696	0.0714
0.1898	0.0694	0.1798	0.0633
0.2100	0.0556	0.1897	0.0504
		0.2001	0.0452
		0.2109	0.0361
		0.2203	0.0362
		0.2291	0.0334
		0.2404	0.0257
		0.2478	0.0196
		0.2589	0.0201

	0.2681	0.0140	

● Tetrahydrofuran Aqueous Solution

Table 11. The mole-fraction dependence of ${}^{SV}\delta_{THF}$ in THF aqueous solution.

x_{THF}	${}^{SV}\delta_{THF}$	x_{THF}	${}^{SV}\delta_{THF}$	x_{THF}	${}^{SV}\delta_{THF}$
0.004984	0.858	0.03002	1.602	0.05512	1.576
0.004990	0.936	0.034915	1.594	0.064895	1.398
0.009959	1.399	0.034975	1.519	0.070075	1.455
0.00997	1.117	0.035005	1.359	0.07501	1.393
0.014920	1.140	0.0371	1.447	0.080045	1.244
0.014964	1.289	0.04501	1.912	0.085175	1.458
0.015003	1.307	0.045025	1.509	0.089915	1.075
0.024825	1.451	0.04707	1.644	0.094795	1.093
0.02495	1.559	0.04989	1.518	0.095285	0.720
0.02499	1.392	0.054995	1.598	0.1049	0.980
0.02507	1.530	0.05512	1.576	0.11485	0.850

● Cyclohexane − Benzene Mixture

Table 12. The mole-fraction dependence of ${}^{SV}\delta_{CZ}$ in Cyclohexane − Benzene Mixture.

x_{CH}	${}^{SV}\delta_{CH}$	x_{CH}	${}^{SV}\delta_{CH}$	x_{CH}	${}^{SV}\delta_{CH}$
0.035	-0.0423	0.375	-0.0166	0.69	-0.0049
0.085	-0.0343	0.425	-0.0142	0.725	-0.0042
0.13	-0.0298	0.475	-0.0120	0.775	-0.0034
0.18	-0.0262	0.52	-0.0101	0.825	-0.0026
0.225	-0.0237	0.57	-0.0083	0.875	-0.0019
0.275	-0.0212	0.62	-0.0067	0.925	-0.0011

0.325	-0.0189	0.66	-0.0056	0.975	-0.0004

(g) Vapor Pressure and Chemical Potential

● p_{vap} in THF Aqueous Solution

Table 13. The mole-fraction dependence of p_{THF} in THF aqueous solution.

x_{THF}	p_{total} / kPa	p_{water} / kPa	p_{THF}/ kPa
0.0000	3.165	3.165	0.000
0.0003	3.293	3.164	0.129
0.0012	3.492	3.162	0.329
0.0024	4.097	3.156	0.941
0.0051	5.026	3.148	1.879
0.0087	6.177	3.138	3.038
0.0130	7.502	3.126	4.376
0.0175	8.730	3.114	5.616
0.0220	9.895	3.102	6.793
0.0265	10.983	3.092	7.891
0.0311	11.964	3.081	8.883
0.0358	12.886	3.070	9.815
0.0424	13.652	3.061	10.591
0.0558	15.599	3.036	12.563
0.0648	16.599	3.022	13.576
0.0827	17.803	3.002	14.800
0.0929	18.418	2.992	15.427
0.1124	19.165	2.976	16.189
0.1353	20.042	2.956	17.087
0.1945	21.077	2.926	18.151
0.2951	21.530	2.908	18.622
0.3962	21.953	2.878	19.074
0.5978	21.956	2.878	19.077
0.6949	22.044	2.853	19.190
0.7969	22.049	2.850	19.198
0.8500	22.110	2.765	19.345
0.9494	22.053	1.473	20.580
1.0000	21.676	0.000	21.676

● μ^{E}_{THF} in THF Aqueous Solution

Table 14. The mole-fraction dependence of μ_{THF} in THF aqueous solution.

x_{THF}	μ^{E}_{THF} / kJ mol^{-1}	x_{THF}	μ^{E}_{THF} / kJ mol^{-1}	x_{THF}	μ^{E}_{THF} / kJ mol^{-1}
0.0003	7.427	0.0311	6.390	0.194	3.619
0.0012	6.341	0.0358	6.294	0.295	2.650
0.0024	7.134	0.0424	6.060	0.396	1.978
0.0051	7.021	0.0558	5.803	0.598	0.959
0.0087	6.905	0.0648	5.625	0.695	0.600
0.0130	6.801	0.0827	5.233	0.797	0.262
0.0175	6.686	0.0929	5.048	0.850	0.121
0.0220	6.587	0.112	4.697		
0.0265	6.493	0.135	4.370		

(h)κ_T

Table 15. The pressure dependence of κ_T in pure water.

323.16 K		313.16 K		303.14 K	
p / MPa	κ_T /10^{-10} Pa^{-1}	p / MPa	κ_T / 10^{-10} Pa^{-1}	p / MPa	κ_T / 10^{-10} Pa^{-1}
1.03	4.414	1.07	4.420	1.02	4.471
5.03	4.368	4.99	4.377	5.01	4.427
10.02	4.312	10	4.321	10	4.372
15.09	4.257	15.08	4.267	14.75	4.320
25.12	4.151	25.11	4.162	25.02	4.211
50.57	3.902	49.73	3.923	50.26	3.963
75.13	3.688	75.34	3.698	75.06	3.741
100.37	3.490	100.18	3.504	100.07	3.541
125.14	3.315	125	3.327	124.97	3.359
150.04	3.156	150.11	3.166	150.03	3.193
175	3.011	175.03	3.020	175.09	3.043
200.16	2.878	200.1	2.887	200.14	2.906
225.31	2.756	224.99	2.765	225	2.781
250.31	2.646	250.14	2.653	249.81	2.668
275.67	2.543	274.99	2.551	275.03	2.562
300.11	2.451	300.25	2.455	300.34	2.464
350.38	2.283	353.74	2.276	350.09	2.293

293.16 K		273.21 K	
p / MPa	κ_T /10^{-10} Pa^{-1}	p / MPa	κ_T / 10^{-10} Pa^{-1}
0.99	4.579	1.14	5.075
5.01	4.533	5.16	5.020
10.04	4.477	10.27	4.948
15.12	4.419	15.06	4.886
25.03	4.312	25.28	4.751
49.96	4.056	50.78	4.426
74.85	3.823	75.12	4.142
100.07	3.610	99.69	3.882
125	3.419	125.25	3.641

150.02	3.244	149.71	3.434
175.1	3.087	175.4	3.241
200.03	2.944	200.2	3.076
225.17	2.813	225.04	2.925
250.12	2.694	249.75	2.791
275.01	2.586	275.41	2.665
300.07	2.486	300.64	2.553
350	2.310	350.42	2.359

(g) $\partial\kappa_T / \partial p$

Table 16. The pressure dependence of $\partial\kappa_T / \partial p$ in pure water.

323.16 K		323.16 K		313.16 K	
p / MPa	$(\partial\kappa_T / \partial p)$ /10^{-19} Pa^{-2}	p / MPa	$(\partial\kappa_T / \partial p)$ /10^{-19} Pa^{-2}	p / MPa	$(\partial\kappa_T / \partial p)$ /10^{-19} Pa^{-2}
3.03	-11.54	3.03	-11.13	3.015	-11.08
7.525	-11.15	7.495	-11.07	7.505	-11.05
12.555	-10.97	12.54	-10.74	12.375	-10.83
20.105	-10.55	20.095	-10.46	19.885	-10.61
37.845	-9.78	37.42	-9.72	37.64	-9.84
62.85	-8.73	62.535	-8.75	62.66	-8.93
87.75	-7.84	87.76	-7.84	87.565	-8.02
112.755	-7.05	112.59	-7.11	112.52	-7.29
137.59	-6.39	137.555	-6.43	137.5	-6.62
162.52	-5.81	162.57	-5.84	162.56	-6.00
187.58	-5.29	187.565	-5.33	187.615	-5.47
212.735	-4.83	212.545	-4.87	212.57	-5.02
237.81	-4.41	237.565	-4.45	237.405	-4.57
262.99	-4.07	262.565	-4.12	262.42	-4.21
287.89	-3.75	287.62	-3.79	287.685	-3.85
325.245	-3.35	326.995	-3.34	325.215	-3.44

323.16 K		323.16 K	
p / MPa	$(\partial\kappa_T / \partial p)$ /10^{-19} Pa^{-2}	p / MPa	$(\partial\kappa_T / \partial p)$ /10^{-19} Pa^{-2}
3	-11.36	3.15	-13.59
7.525	-11.23	7.715	-14.17
12.58	-11.26	12.665	-12.85
20.075	-10.83	20.17	-13.24
37.495	-10.26	38.03	-12.73
62.405	-9.37	62.95	-11.70
87.46	-8.47	87.405	-10.57
112.535	-7.66	112.47	-9.42
137.51	-6.96	137.48	-8.48
162.56	-6.29	162.555	-7.52

187.565	-5.72	187.8	-6.65
212.6	-5.21	212.62	-6.07
237.645	-4.75	237.395	-5.43
262.565	-4.35	262.58	-4.91
287.54	-3.98	288.025	-4.43
325.035	-3.54	325.53	-3.89

(h)$\partial^2\kappa_T / \partial p^2$

Table 17. The pressure dependence of $\partial^2\kappa_T / \partial p^2$ in pure water.

	273 K	293 K	303 K	313 K	323 K
p / MPa	$(\partial^2\kappa_T / \partial p^2)$ / 10^{-18}Pa^{-3}	$(\partial^2\kappa_T / \partial p^2)$ / 10^{-18}Pa^{-3}	$(\partial^2\kappa_T / \partial p^2)$ / 10^{-18}Pa^{-3}	$(\partial^2\kappa_T / \partial p^2)$ / 10^{-18}Pa^{-3}	$(\partial^2\kappa_T / \partial p^2)$ / 10^{-18}Pa^{-3}
10	0.00465	0.0037	0.00385	0.0045	0.0048
30	0.00455	0.0036	0.00385	0.0043	0.00465
50	0.00455	0.0036	0.00375	0.0038	0.00425
70	0.00445	0.00335	0.0036	0.00365	0.00385
90	0.00435	0.00325	0.0032	0.00325	0.0033
110	0.00415	0.00295	0.0029	0.003	0.00305
130	0.00385	0.00285	0.00275	0.00265	0.00265
150	0.00375	0.0026	0.00255	0.0024	0.00245
170	0.00325	0.00235	0.00215	0.00205	0.00205
190	0.003	0.0022	0.00195	0.00185	0.0019
210	0.0026	0.00195	0.0019	0.00175	0.0017
230	0.0023	0.00175	0.00155	0.0015	0.00155
250	0.00205	0.00165	0.0015	0.0015	0.00135
270	0.0019	0.00145	0.0013	0.0013	0.0013
290	0.0017	0.0014	0.0013	0.0012	0.00115
310	0.0015	0.0012	0.001	0.00105	0.0011
330	0.0015	0.0011	0.001	0.00105	0.001

VII. Appendix – List of Publications

1. Acceleration of the effect of solute on the entropy-volume cross fluctuation density in aqueous 2-butoxyethanol, 1-propanol, and glycerol: The fourth derivative of Gibbs energy.

   K. Yoshida, S. Baluja, A. Inaba, Y. Koga. *J. Chem. Phys*. **2011**, *134*, 214502.

2. Experimental Determination of a Third Derivative of G. (III): Differential Pressure Perturbation Calorimetry (II).

   K. Yoshida, S. Baluja, A. Inaba, K. Tozaki, Y. Koga, *J. Solution Chem.* **2011**, *40*, 1271–1278.

3. Anomalies in the Third Derivatives of Gibbs Energy and Their Temperature Dependence in Aqueous 2-Butoxyethanol and Glycerol: On the so Called Koga Lines.

   K. Yoshida, A. Inaba, Y. Koga, *J. Solution Chem.* **2014**, *43*, 663-674.

4. Gradual Crossover in Molecular Organization of Stable Liquid H_2O at Moderately High Pressure and Temperature.

   Y. Koga., Westh, P., Yoshida, K., Inaba, A., Nakazawa, Y. *AIP Adv.* **2014**, *4*, 097116.

5. Third derivative thermodynamic quantities of aqueous tetrahydrofuran at 25° C

   K. Yoshida, P. Westh, A. Inabaa, M. Nakanoa, Y. Koga, *J. Mol. Liq.*, **2014**, *43*, 40-45.